The Pennsylvania State University

The Graduate School

Department of Materials Science and Engineering

TEMPERATURE DEPENDENCE OF DIELECTRIC BREAKDOWN IN POLYMERS

A Thesis in

Materials Science and Engineering

by

Cheolhong Min

Submitted in Partial Fulfillment
of the Requirements
for the Degree of

Master of Science

August 2008

The thesis of Cheolhong Min was reviewed and approved* by the following:

Thomas R. Shrout
Professor of Materials Science
Thesis Co-Advisor

Michael T. Lanagan
Associate Professor of Engineering Science and Mechanics
Thesis Co-Advisor

Shujun Zhang
Research Associate and Assistant Professor of Materials Science and Engineering

Joan Redwing
Professor of Materials Science and Engineering
Chair, Intercollege Graduate Degree Program in Materials Science and Engineering

*Signatures are on file in the Graduate School

ABSTRACT

Capacitors possess high-power densities and have the ability to deliver energy with short discharge times, which are in the micro-second to nano-second range. Both energy and power density are related to the dielectric materials used in the capacitor. One of the main challenges for capacitors is achieving high energy density as determined by the relative permittivity and dielectric breakdown strength of a material. Polymers are some of the most important dielectric materials for high-power capacitors because polymer films show high breakdown strength. A general trend in polymers is that the breakdown strength increases with decreasing temperature. An understanding of the temperature dependence relationships among electrical properties, polymer chemistry, and crystalline structure may lead to improved energy storage for polymer-based capacitors—this is the basis of the thesis.

Various polymers including polypropylene (PP), polyimide (PI), polymethyl methacrylate (PMMA), poly(vinylidene fluoride-trifluoroethylene-chlorotrifluoroethylene) terpolymer (p(VDF-TrFE-CTFE)) were investigated in this study. Electrical properties of the polymers including low-field ($<1X10^{-3}$MV/mm) permittivity (ε_r), dielectric loss ($\tan\delta$), high-field (>1MV/cm) permittivity, and dielectric breakdown strength will be discussed. Temperature dependence of low-field permittivity, dielectric loss, and dielectric breakdown in the polymers is also presented. The electrical properties of the polymers have been investigated over a temperature range from -196°C to 170°C. Breakdown strength (E_{Br}) of all the polymers was found to decrease with increasing temperature. Maximum energy per unit volume (E_{vol}) of the various polymers at maximum breakdown strength is also introduced using relative permittivity.

TABLE OF CONTENTS

LIST OF FIGURES vi

LIST OF TABLES ix

ACKNOWLEDGEMENTS x

Chapter 1 Introduction 1

Chapter 2 Dielectric Breakdown in Polymer Dielectrics 10

2.1 Introduction 10
2.2 Electrical Breakdown Mechanisms 12
2.2.1 Electronic Breakdown 12
2.2.1.1 Intrinsic Breakdown 12
2.2.1.2 Avalanche Breakdown 15
2.2.2 Thermal Breakdown 17
2.2.3 Electromechanical Breakdown 19
2.3 Structure of Polymer Dielectrics 25
2.3.1 Glass-transition Temperature 25
2.3.2 Crystallinity 26
2.3.3 Cohesive Energy Density related to Dielectric Breakdown in Polymers 27

Chapter 3 Experimental Approach 31

3.1 Introduction 31
3.2 Materials 33
3.2.1 Polypropylene (PP) 33
3.2.2 Polyimide (PI) 34
3.2.3 Polymethyl Methacrylate (PMMA) 35
3.2.4 P(VDF-TrFE-CTFE) Terpolymer 36
3.3 Film Preparation 38
3.3.1 Polymer Films 39
3.4 Relative Permittivity and Dielectric-Loss Measurements 40
3.5 Dielectric-Displacement Measurements 41
3.6 Breakdown Measurements 43

Chapter 4 Experimental Results and Discussion 49

4.1 Introduction 49
4.2 Low Field Permittivity and Dielectric Loss 49
4.2.1 Relative Permittivity and Dielectric Loss at Room Temperature 50

4.2.2 Temperature Dependence of Relative Permittivity and Dielectric Loss 51
4.3 High-field Permittivity 56
4.4 Dielectric Breakdown in Polymers 57
4.4.1 Dielectric Breakdown of Polymer Films at Room Temperature 58
4.4.2 Temperature Dependence of the Breakdown Strength of Polymer Films 60
4.5 Energy Density 66

Chapter 5 Conclusion and Future Work 69

5.1 Conclusion 69
5.2 Future Work 71

LIST OF FIGURES

Figure **1.1**: Power density vs. energy density for various energy storage components. Capacitors possess high-power densities as a result of a short discharging time [1] 2

Figure **1.2**: Frequency dependence of dielectric permittivity. Dielectric permittivity (ε_r') and loss (ε_r'') are affected by frequency [5] 4

Figure **1.3**: P-E of (a) a linear dielectric material and (b) a ferroelectric material that exhibits a hysteretic non-linear response 5

Figure **1.4**: Comparison of energy density for various dielectric materials for high-power capacitors. Energy density is limited by dielectric permittivity and the electric field due to breakdown strength of a material. 1) biaxially oriented PP, 2) modified poly(vinylidene fluoride) polymer, 3) titanium oxide dielectric, 4) antiferroelectric/ferroelectric phase switch ceramic, 5) PP film capacitor, 6) PVDF film capacitor, 7, 8) ceramic capacitors, 9) commercial polymer film power capacitor [6] 6

Figure **1.5**: Temperature dependence of electric strength in polymer dielectrics. The electric strength increased with decreasing temperature [7] 7

Figure **2.1**: Mechanisms of time to breakdown and breakdown strength (E_{Br}) when breakdown occurs [1] 11

Figure **2.2**: Partial discharge when an electric field is applied to (a) a void of a dielectric material, and (b) a crack between the dielectric material and a metallic electrode [1] 11

Figure **2.3**: Fröhlich's energy band model. It is assumed that a trap band is directly below a conduction band [2] 14

Figure **2.4**: Thickness-dependent DC breakdown strength in LDPE films at -196°C [5]. 17

○: blank, ⊙: 1wt% pyrene doped, ●: 1wt% AS-1 doped 17

Figure **2.5**: Time backward from breakdown dependence of current before breakdown of PI at 90°C [6] 19

Figure **2.6**: Electrostatic force is induced between electrodes when an electric field is applied to the electrodes [1] 20

Figure **2.7**: Normalized thickness of a rubbery material as a function of normalized voltage [2] 22

Figure **2.8**: Outline of the temperature dependence of breakdown strength in linear polymers [4] 24

Figure **2.9**: Five regions of viscoelasticity depending on temperature for polystyrene (PS). Relaxation modulus of PS varies with temperature [8] 24

Figure **2.10**: Correlation between breakdown strength and cohesive energy-density in polar/non-polar polymers [2, 13, 14] 27

Figure **2.11**: Correlation between breakdown strength (E_b) and cohesive-energy density (CED) with changing temperature for low-density polyethylene (LDPE). The solid line indicates the cohesive-energy density, and the symbols define the breakdown strength [2] 28

Figure **3.1**: Chemical structure of PP. A methyl group is bonded with a carbon of a propylene monomer. The orientation of the methyl groups defines tacticity in PP 34

Figure **3.2**: Chemical structure of polyimide (PI). The chemical structure of the polyimide is derived from polyamic acid [23] 34

Figure **3.3**: Chemical structure of polymethyl methacrylate (PMMA). A monomer of PMMA contains a methyl and a methacrylic group. The tacticity of PMMA chains is defined by the orientation of the groups 35

Figure **3.4**: Chemical structure of p(VDF-TrFE-CTFE) terpolymer. CTFE is introduced into the p(VDF-TrFE) copolymer. Properties of the terpolymer vary with changing chemical composition 36

Figure **3.5**: TrFE concentration dependence of breakdown strength and storage modulus for p(VDF-TrFE-CTFE) terpolymer [15] 37

Figure **3.6**: Electrode configurations for measurements of electrical properties including (a) breakdown (b) relative permittivity, dielectric loss, and dielectric displacement 39

Figure **3.7**: Experimental setup for relative permittivity and dielectric-loss measurements [26] 41

Figure **3.8**: Experimental setup for dielectric-displacement and -breakdown measurements. Temperatures were maintained for the breakdown measurements [27] 42

Figure **3.9**: Modified Sawyer-Tower circuit at 1.5MV/cm–6.5MV/cm, 10Hz, and room temperature. In P-E, a linear dielectric shows a linear response, and a ferroelectric material exhibits a non-linear response [27, 29] 43

Figure **3.10**: Two sample holders including (a) trough holder and (b) mushroom holder used for breakdown-strength measurements 45

Figure **4.1**: Temperature dependence of low-field (a) permittivity (ε_r) and (b) dielectric loss (tanδ) of PP films 52

Figure **4.2**: Temperature dependence of low-field (a) permittivity (ε_r) and (b) dielectric loss (tanδ) in PI 53

Figure **4.3**: Temperature dependence of low-field (a) permittivity (ε_r) and (b) dielectric loss (tanδ) of PMMA 54

Figure **4.4**: Temperature dependence of low-field (a) permittivity (ε_r) and (b) dielectric loss (tanδ) of p(VDF-TrFE-CTFE) terpolymer 55

Figure **4.5**: Dielectric displacement of various polymer films including (a) PP, (b) PI, (c) PMMA, and (d) p(VDF-TrFE-CTFE) terpolymer at room temperature ... 57

Figure **4.6**: Weibull distribution of breakdown in various polymer films at room temperature including (a) PP, (b) PI, (c) PMMA, and (d) p(VDF-TrFE-CTFE) terpolymer 60

Figure **4.7**: Differential scanning calorimetry (DSC) data for PI with various water contents [17] 63

Figure **4.8**: Thermogravimetric analysis (TGA) data for PI which shows a change in weight percent with changing temperature 64

Figure **4.9**: Temperature dependence of breakdown strength in various polymer films including (a) PP, (b) PI [14], c) PMMA, and (d) p(VDF-TrFE-CTFE) terpolymer. Circles (○) indicate breakdown data using liquid nitrogen 65

Figure **5.1**: Normalized breakdown strength of various polymer films including (a) PP, (b) PI [2], (c) PMMA, and (d) P(VDF-TrFE-CTFE) terpolymer 71

Figure **5.2**: Experimental setup for low-temperature breakdown measurements [2]... 72

Figure **5.3**: Design of optimum polymers to enhance energy density 73

LIST OF TABLES

Table **3.1**: General properties of various polymers including PP, PMMA, PI, and p(VDF-TrFE-CTFE) terpolymer [1-16] 32

Table **3.2**: Various compositions and degrees of crystallinity for p(VDF-TrFE-CTFE) terpolymer [15] 38

Table **3.3**: Thickness and electrode material for the various polymer films. The thickness of electrodes was about 50nm 39

Table **3.4**: Insulating media for the investigation of temperature dependence of dielectric breakdown in various polymer films. (BP: boiling point, MP: melting point, SP: sublimation point) [30–32] 44

Table **4.1**: Comparison of relative permittivity (ε_r) and dielectric loss ($\tan\delta$) for the various polymer films at room temperature 51

Table **4.2**: Room temperature breakdown strengths of the various polymer dielectrics 59

Table **4.3**: Maximum energy density of various polymers at the maximum breakdown strength 66

Table **5.1**: Electrical properties of various polymer dielectrics 70

ACKNOWLEDGEMENTS

First of all, this investigation was supported by the Republic of Korea Army through their study abroad program for Army officers and by the Office of Naval Research under the MURI (multidisciplinary university research initiative) program.

I am very grateful to my advisors, Dr. Tom Shrout and Dr. Mike Lanagan, and to committee member, Dr. Shujun Zhang, for their support, kindness, and invaluable advice throughout my days at The Pennsylvania State University.

I would like to thank all the members in our group, especially Beth Jones for supporting the experimental instruments necessary for my research. My office mates, Roni Levi, Patamas Bintachitt, and Raegan Johnson, were always generous with advice and assistance for which I also give many thanks.

I would also like to thank my friends, the staff and faculty members, at the Materials Research Laboratory, the Steidle Building, the Department of Materials Science and Engineering, and the College of Earth and Mineral Sciences. In particular, I must mention Youmi Jeong, who helped me immensely through our many discussions of polymer chemistry: in working with me to find the right experimental approach to my work, he brought both patience and considerable insight. Dokyun Kwon showed me the in terms of conducting my investigations, and in doing so helped me to negotiate my first year of study. Soonil Lee, Jeongryeol Kim, Hyeran Noh, Jongbong Lim, and Hoikwan Lee were always made themselves available to troubleshoot my experiments and my results. Eugene Furman always offered me commentary about my results that never failed to move my research forward. Guneet Sethi discussed many issues pertinent to my

research with me and also offered practical assistance by making oxide/polymer composites for me. Badri Rangarajan and Pratyush Tewari also spent much time with me, discussing my results in the collegial spirit so useful and supportive to all researchers, especially Pratyush Tewari for carrying out thermogravimetric analysis (TGA) data for polyimide (PI). Jeff Long and Paul Moses (dielectric measurement), Maria DiCola (sputtering), Nichole Wonderling (XRD), Maria Klimkiewicz (SEM), Chiping Wang (breakdown), Amanda Baker (profilometer) and Xin Zhou (evaporating) also played a role in helping me obtain good results. Joanne Aller, Donna Lucas, Michelle Hill, and Kathy Gummo rendered valuable service by helping me improve my papers. For questions about polymers, I turned to Jason Claude and Bret Neese. Hyunjae Kim, Pilyeon Park, Sunghoon Lee, Youngho Jin, Uhyeok Choi, Yuichi Matsuyama, Ichiro Fujii, Joseph Scholz, and Vivek Tomer were always there when I needed a friend; their support and kindness also helped to deal with the madness that sometimes characterizes State College. In addition, Jincheol Ryu, Jinhyun Park, Sunam Ryu, Sunyoung Park, Jungmok Ma, and their wives took good care of me like their family.

Finally, special thanks go to my parents, Kyungbaek Min and Juheung Lee, and my younger sister, Ahri Min. They have always encouraged, and emotionally and spiritually supported me to accomplish my educational and career goals.

I could not have finished this thesis without the great many people mentioned here, as well as some who are not; their support, collegiality, and kindness did much to make my two years at Penn State successful—a time I will look back on as both personally and professionally fulfilling.

Chapter 1

Introduction

There are many energy-storage components including batteries, supercapacitors, electrolytic capacitors, and solid-state capacitors. These components possess different power and energy densities as depicted in Figure **1.1**. Fuel cells and batteries exhibit high-energy densities with low-power densities. Capacitors possess high-power densities with low-energy densities. The ability of short discharge times below 0.01 seconds in solid-state capacitors results in a high-power density [1]. Capacitor components have the highest power density among all of the devices shown in Figure **1.1**. Supercapacitors rely on charge transport through liquid media and have higher energy densities than solid-state capacitors. The supercapacitors use special electrodes, including high-surface-area-activated carbons, metal oxides, and conducting polymers [2]. Electrolytes including aqueous and/or organic may also be used for electrolytic capacitors [2]. One of the disadvantages of supercapacitors in relation to solid-state capacitors is the low cell voltages of the supercapacitors [3]. Solid-state capacitors are used for sources of charge switch devices, AC/DC power conversion, etc., [4]. The primary limitation for solid-state capacitors is energy density, which is significantly lower than other energy storage and conversion devices. As stated, solid-state capacitors offer high-power densities as shown in Figure **1.1**.

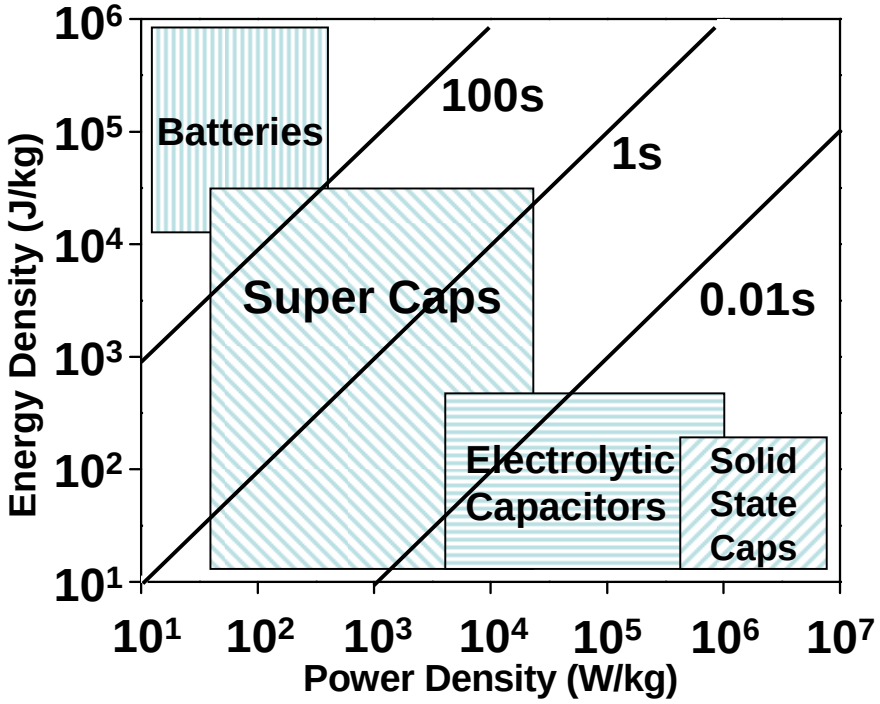

Figure **1.1**: Power density vs. energy density for various energy storage components. Capacitors possess high-power densities as a result of a short discharging time [1]

There are several important material parameters for assessing dielectrics including permittivity (ε), DC resistivity (ρ), dielectric loss (tan δ), and temperature stability. The capacitance, loss, and resistance values are directly related to the dielectric material's properties. Capacitance is related to the dielectric permittivity when a dielectric is located between parallel electrodes, and the capacitance is given in Equation **1.1**.

$$C = \varepsilon_r \varepsilon_o \frac{A}{d} \qquad \text{Equation } \mathbf{1.1}$$

where, ε_o is the permittivity of free space (8.8542 X 10^{-12} F/m), A is the effective area of the dielectric, and d is the thickness of the dielectric.

The loss tangent, tanδ, is defined by the real part of the complex relative permittivity, ε_r', and the imaginary part of the complex relative permittivity, ε_r'', as stated in Equation **1.2**. Undesirable dielectric heating increases with increasing dielectric loss.

$$\tan\delta = \frac{\varepsilon_r''}{\varepsilon_r'} \qquad \text{Equation } \mathbf{1.2}$$

Insulation resistivity (ρ) is related to the DC resistance (R), thickness, and area of the dielectric, as expressed in Equation **1.3**.

$$\rho = \frac{RA}{d} \qquad \text{Equation } \mathbf{1.3}$$

The insulation resistivity, ρ, and the dielectric permittivity, ε, are fundamental material parameters. DC resistance and capacitance can be expressed as a dimensionless quantity using dielectric permittivities and insulation resistivity, as given in Equation **1.4**.

$$RC = \varepsilon_r \varepsilon_o \rho \qquad \text{Equation } \mathbf{1.4}$$

A dielectric shows various polarization mechanisms including interfacial, orientational, ionic, and electronic polarizations. The real and imaginary parts of the complex relative permittivity are dependent on frequency as depicted in Figure **1.2**. Dielectric permittivity displays a decrease when a polarization mechanism is induced at a frequency. Dielectric loss shows the highest value when polarization frequency is the same as lattice vibration frequency because energy is dissipated by the lattice vibration [5].

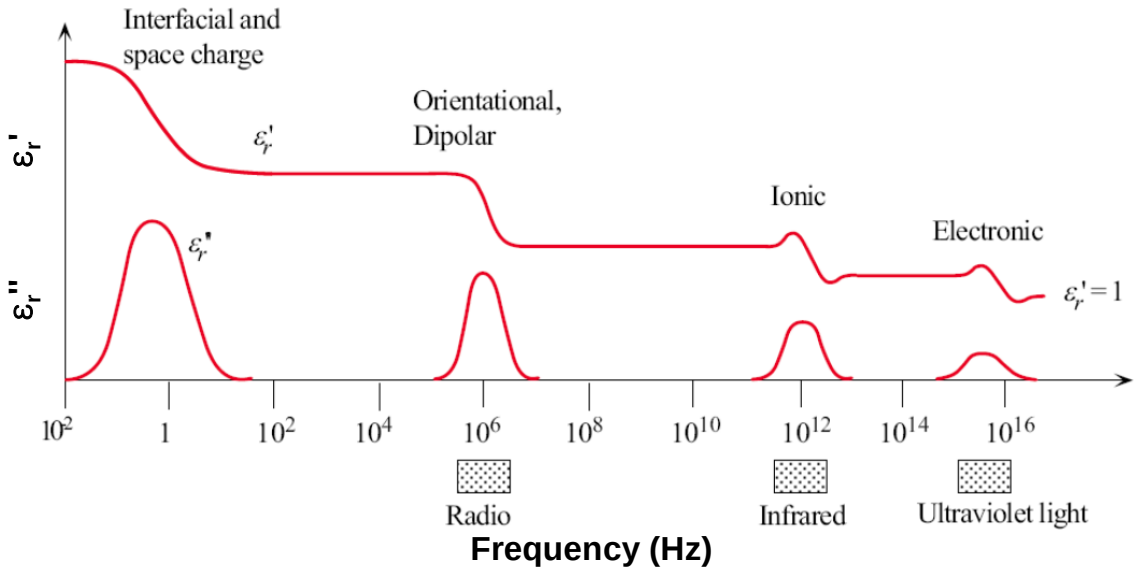

Figure **1.2**: Frequency dependence of dielectric permittivity. Dielectric permittivity (ε_r') and loss (ε_r'') are affected by frequency [5]

Examples of P-E behavior are given in Figure **1.3**. If an electric field is applied to a linear dielectric material such as polymers, e.g., polypropylene or polyimide, the polarization-electric field (P-E) will show a linear response as depicted in Figure **1.3** (a). The dielectric displacement is directly proportional to the applied electric field. The integrated triangular area is related to the stored energy in the dielectric. If an electric field is applied to a ferroelectric material, a polarization will remain after removing the electric field and P-E will show a hysteretic non-linear response like (b). Relative permittivity (ε_r) of a material is indicated from a slope of P-E as given in Equation **1.5**.

$$P = \varepsilon_o \varepsilon_r E \qquad \text{Equation } \mathbf{1.5}$$

The dielectric loss ($\tan\delta$) over the charge/discharge cycle is related to the area within the hysteresis loop. Ferroelectric materials show higher dielectric loss than linear

dielectric materials due to the higher dipole moment of the ferroelectric materials. The energy density (U_e) of a material is derived from the integrated triangular area of the loop.

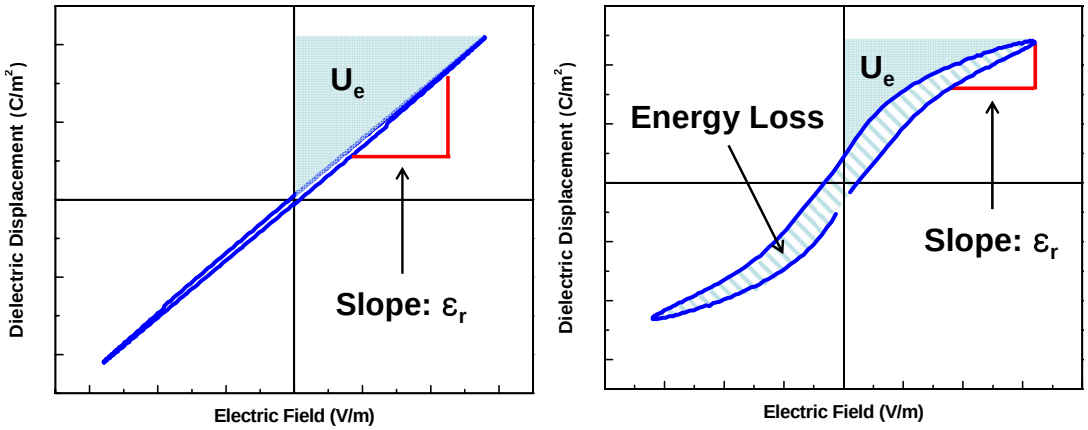

Figure **1.3**: P-E of (a) a linear dielectric material and (b) a ferroelectric material that exhibits a hysteretic non-linear response

The energy density (U_e) of a capacitor is the integrated area of P-E. The energy density is expressed in Equation **1.6**.

$$U_e = \int EdD \qquad \text{Equation } \mathbf{1.6}$$

The maximum energy stored per unit volume (E_{vol}) is related to dielectric permittivity and breakdown strength (E_{Br}) as given in Equation **1.7**.

$$E_{vol} = \frac{1}{2}\varepsilon_o \varepsilon_r {E_{Br}}^2 \cong \frac{1}{2} C V_m^2 \times \frac{1}{Ad} \qquad \text{Equation } \mathbf{1.7}$$

where, V_m is the maximum voltage, A is the area of the capacitor plates, and d is the separation of the capacitor plates.

Energy density comparisons in relation to dielectric permittivities and the electric field of various dielectrics are depicted in Figure **1.4**. High-energy density can be achieved by increasing the relative permittivity or the dielectric breakdown strength of a

material. Polymer dielectrics generally have lower permittivity than ceramic dielectrics, e.g., TiO_2 and $BaTiO_3$. Polymer dielectrics including PP (polypropylene) and PMMA (polymethyl methacrylate) possess relative permittivity values in the 2 to 4 range. In order to achieve energy densities in excess of 5J/cc, dielectric breakdown fields would have to exceed $5X10^8$ V/m.

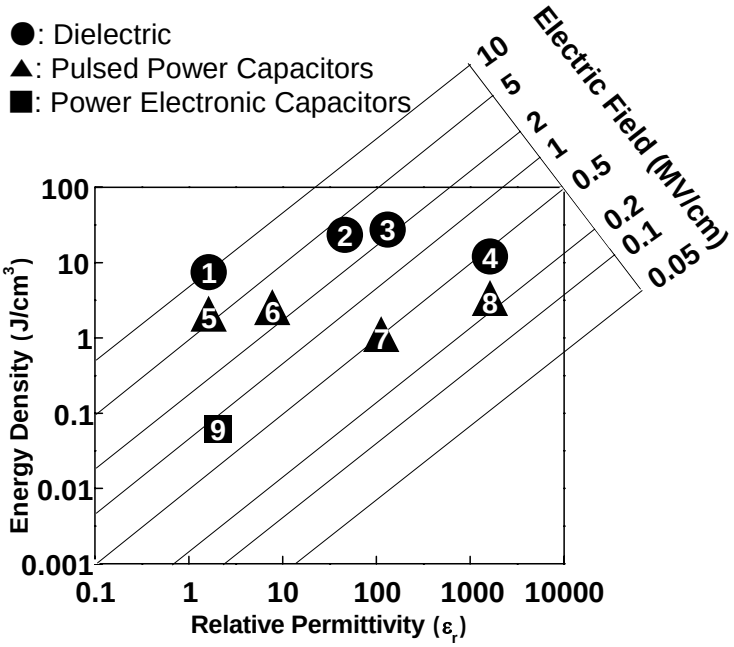

Figure **1.4**: Comparison of energy density for various dielectric materials for high-power capacitors. Energy density is limited by dielectric permittivity and the electric field due to breakdown strength of a material. 1) biaxially oriented PP, 2) modified poly(vinylidene fluoride) polymer, 3) titanium oxide dielectric, 4) antiferroelectric/ferroelectric phase switch ceramic, 5) PP film capacitor, 6) PVDF film capacitor, 7, 8) ceramic capacitors, 9) commercial polymer film power capacitor [6]

Polymers are some of the most important dielectric materials for high-power capacitors. Polymer films show high breakdown strength as shown in Figure **1.4**. A general trend in polymers is that breakdown strength increases with decreasing temperature. The strong dependence on temperature is depicted in Figure **1.5** for standard

polymer dielectrics. Polar polymers including PVA (polyvinyl alcohol), PMMA (polymethyl methacrylate), and PVC-Ac (polyvinyl chloride-acetate) exhibit a strong temperature dependence in regard to dielectric breakdown strength than non-polar polymers including PS (polystyrene), LDPE (low-density polyethylene), and PIB (polyisobutylene). Some polymers show an abnormal change in breakdown strength with changing temperature. An understanding of the relationships among temperature dependence, polymer chemistry, and crystalline structure may lead to improved energy storage for polymer-based capacitors—which is the basis of this thesis.

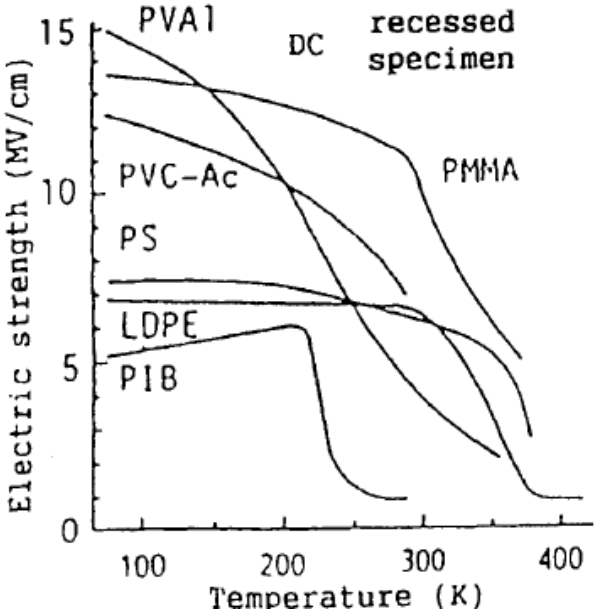

Figure **1.5**: Temperature dependence of electric strength in polymer dielectrics. The electric strength increased with decreasing temperature [7]

In the following chapters, various polymers including polypropylene (PP), polyimide (PI), polymethyl methacrylate (PMMA), poly(vinylidene fluoride-trifluoroethylene-chlorotrifluoroethylene) terpolymer (p(VDF-TrFE-CTFE)) were investigated in this study, and the temperature-dependent dielectric properties and

breakdown strengths will be introduced. Low-field (<1X10^{-3}MV/cm) permittivity (ε_r) and dielectric loss (tanδ) of the polymers with changing temperature were calculated from capacitance measurements. High-field permittivity (>1MV/cm) was calculated from dielectric displacement measurements. Dielectric breakdown data of the polymers was statistically analyzed using Weibull distribution. Temperature dependence of dielectric breakdown in the polymers will be discussed. Various breakdown mechanisms in relation to temperature were also studied and related to polymer chemistry and structure, including temperature-related phenomena. It is carried out to evaluate potential uses of polymer dielectrics in high-energy capacitors.

References

1. T. Christen, M.W. Carlen, Theory of Ragone Plots, Journal of Power Sources, 91, 210-216 (2000)
2. I. Buchmann, What's the Role of the Supercapacitor?, http://www.batteryuniversity.com/partone-8.htm, (2003)
3. T. Wei, S. Wang, and Z. Qi, Design of supercapacitor based ride through system for wind turbine pitch systems, Proceedings of the Electrical Machines and Systems, 2007. ICEMS. International Conference, 294-297 (2007)
4. A.J. Turo, Dielectric Studies in Materials for High Energy Density Capacitors, Trident Scholar Project Report; No. 361, US Naval Academy (2007)
5. S.O. Kasap, Principles of Electronic Materials and Devices, 3rd ed, McGraw-Hill (2005)
6. M. Lanagan, T. Shrout, B. Rangarajan, S. Perini, S. Conzone, and C. Pantano, Glass-based dielectrics for High Temperature Capacitors, Proceedings of the High Temperature Electronics, Albuquerque, NM, (2008)
7. M. Ieda, M. Nagao, and M. Hikita, High-field Conduction and Breakdown in Insulating Polymers, IEEE Transactions on Dielectrics and Electrical Insulation, 1, 934-945 (1994)

Chapter 2

Dielectric Breakdown in Polymer Dielectrics

2.1 Introduction

Polymers are generally excellent dielectric materials for high-voltage energy storage. As with all dielectrics, however, there are limitations in voltage and the electric field in which dielectric breakdown occurs. Solid-state materials are damaged permanently and a continuous conducting path is formed when dielectric breakdown is introduced. Dielectric breakdown of solids is affected by molecular structure, defects, properties of electrodes, temperature, conditions of atmosphere, and applied frequency, etc., [1]. In addition, dielectric breakdowns under DC and/or AC fields vary significantly.

Understanding the fundamental dielectric breakdown of polymers is difficult because of the large number of mechanisms as depicted in Figure **2.1**. The particular type of mechanism is governed by time to breakdown. For example, in electrochemical breakdown, water trees develop through a kinetically limiting chemical reaction that may take many days. Partial discharge from voids takes place in the time frame of seconds to an hour, and it is caused by discharge in a weak area of the dielectric as shown in Figure **2.2**.

The focus of this thesis is the short-term dielectric breakdown (< 0.1 second) in which intrinsic, avalanche, thermal, electromechanical breakdown mechanisms are relevant [1]. Most of the polymers in this study have breakdown strengths exceeding

1MV/cm, and the thermal, electromechanical, and intrinsic breakdown mechanisms are the most relevant.

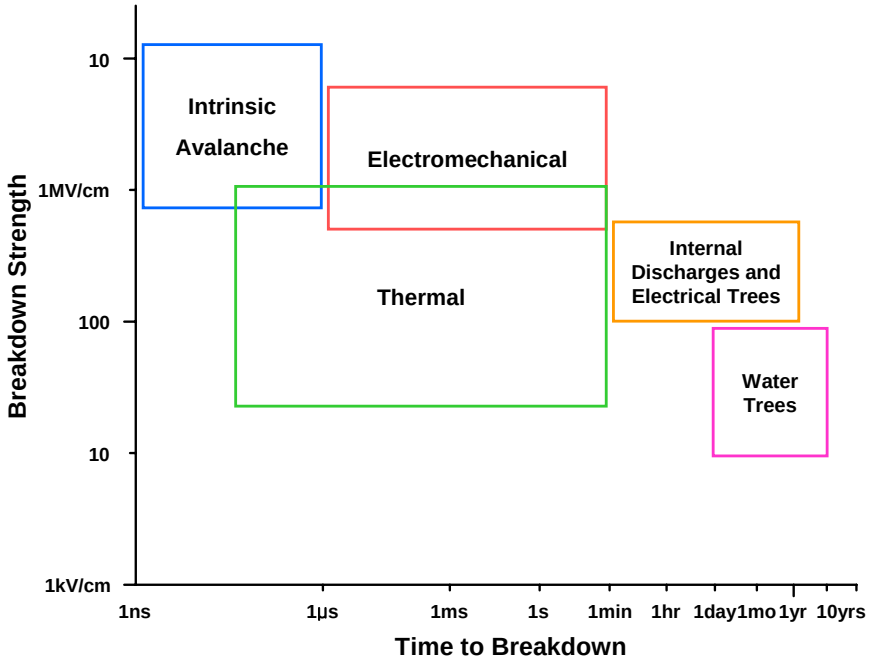

Figure **2.1**: Mechanisms of time to breakdown and breakdown strength (E_{Br}) when breakdown occurs [1]

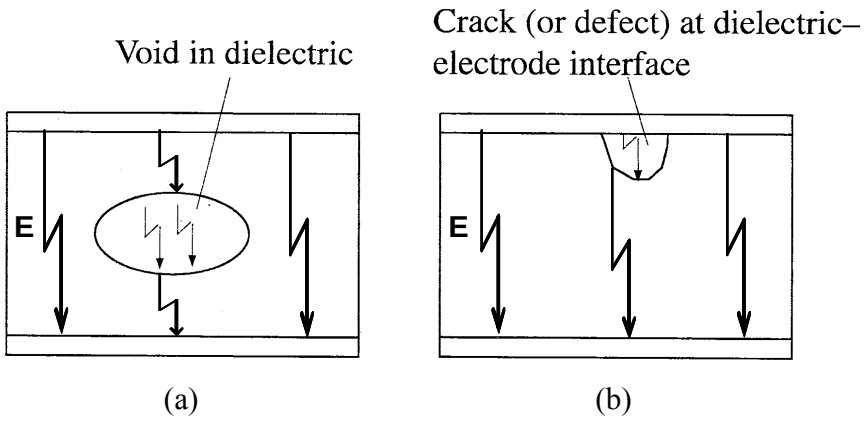

Figure **2.2**: Partial discharge when an electric field is applied to (a) a void of a dielectric material, and (b) a crack between the dielectric material and a metallic electrode [1]

2.2 Electrical Breakdown Mechanisms

Many potential dielectric breakdown mechanisms of polymers depend on intrinsic and extrinsic aspects of the dielectrics [1]. Intrinsically, the band gap and bond strength are important material properties. Extrinsic defects that create free electronic or ionic charge reduce the breakdown field from intrinsic values. Mechanical properties also play a role in determining dielectric breakdown strength. This section will summarize the most important mechanisms for high-quality polymers for pulse-power capacitor applications.

2.2.1 Electronic Breakdown

Electronic breakdown processes generally involve the acceleration of free electrons that gain sufficient energy to ionize a host atom within the dielectric material. The high-energy free electrons are available from the conduction band or injected from the metal contact. For both intrinsic and avalanche breakdown processes, high-electric fields will generate free electrons and give energy to them in an electronic breakdown process.

2.2.1.1 Intrinsic Breakdown

A power balance governs electron energy and, therefore, ultimately controls intrinsic breakdown. Free electrons gain energy in a high-electric field and lose their energy by electron-phonon scattering [2]. Breakdown occurs if the rate of energy gain exceeds the rate of energy loss. This mechanism is intrinsic breakdown. Additional

electron energy-loss mechanisms include inelastic collisions by defects and scattering between electrons, which are not considered in the intrinsic power balance [2].

A power balance in intrinsic breakdown is quantified by Equation **2.1** and Equation **2.2**. The power balance is related to the energy gain and loss of electrons [2].

$$A(E, T, \alpha)=B(T, \alpha) \qquad \text{Equation } \mathbf{2.1}$$

where A is the rate of energy gain, B is the rate of energy loss, E is the applied electric field, T is temperature, and α is electron energy bands.

$$A=\frac{JE}{n} \qquad \text{Equation } \mathbf{2.2}$$

where J is the current density ($J=\sigma E$, σ is electrical conductivity) and n is the number of free electrons. The rate of energy gain is dependent on the applied electric field. J and n are dependent on temperature. The general power balance equation is given in Equation **2.3**.

$$\frac{dT}{dt}=\frac{1}{C_p D}(\sigma E^2+\kappa\nabla^2 T) \qquad \text{Equation } \mathbf{2.3}$$

where C_p is specific heat, D is density, and κ is thermal conductivity. Breakdown does not occur if $dT/dt=0$ at $T<T_c$ (T_c is the critical temperature). But, if either $dT/dt=\infty$ or $T=\infty$ or $T=T_c$ breakdown will occur [2].

Von Hippel regarded a single average electron in the conduction band as sufficient to explain intrinsic breakdown [3]. The interaction between electrons was neglected in the theory. An electron gains energy from the applied electric field. The gained energy is dissipated to the lattice by electron-phonon scattering. Breakdown is

introduced when the energy gain is higher than the energy loss, which is due to lattice collisions [2].

In most experimental results, electric strength decreases as temperature increases. For example, this behavior is shown in amorphous or impure solids that have additional electron energy states. Those solids have centers that can increase electron scattering [3]. Electrons are in the trap band (ΔE), which is exited under the conduction band as depicted in Figure **2.3** [2]. Electron–electron collisions occur between trapped electrons in the trap band and conduction band. Trapped electrons in the trap band are coupled to conduction electrons because of inter-electron collisions. These trapped electrons influence energy loss. This behavior contributes to the decrease of electric strength with increasing temperature, which, in turn, increases electron energy. This theory can be applied to amorphous or impure materials because those materials have centers that increase electron scattering [3].

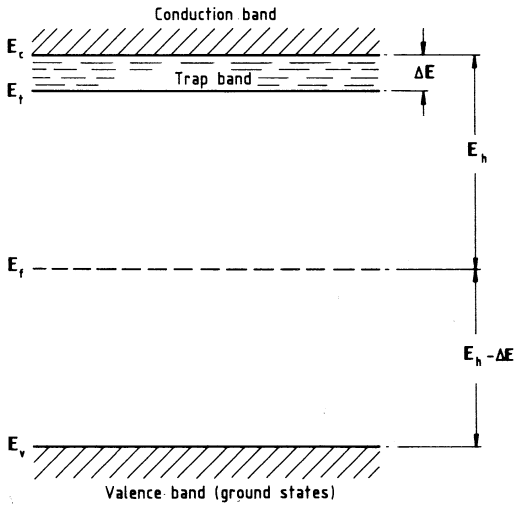

Figure **2.3**: Fröhlich's energy band model. It is assumed that a trap band is directly below a conduction band [2]

In the energy-loss process, electron temperature (T_e) has to be higher than the lattice temperature (T_o). The breakdown field is defined with temperature as given in Equation **2.4** [2].

$$E_{br} = \frac{c}{\sqrt{\Delta E}} \exp\left(\frac{\Delta E}{2kT_e}\right) \qquad \text{Equation } \mathbf{2.4}$$

where c is a constant defined by Fröhlich that is related to the frequency of lattice scattering, ΔE is the bandwidth of shallow trap states, and k is the Boltzmann constant.

This theory predicts that electric strength decreases as temperature increases. For polymer dielectrics, polar groups and defects increase electric strength at low temperature because they act as additional traps [2]. Co-monomers in co-polymers also increase electric strength because co-monomers act as electron traps that decrease high-field conductivity [2]. Ieda explained the increase of electric strength in co-polymers. Polyethylene is co-polymerized with PBPM (pentabromophenyl methacrylate), TBPM (tribromophenyl methacrylate). These halogen co-monomers act as electron traps. Electric strength increases with decreasing high-field conductivity because of the action of co-monomers [2].

2.2.1.2 Avalanche Breakdown

Avalanche breakdown is a general mechanism of dielectric breakdown. A free electron of a dielectric has enough energy to collide with other electrons or ionize an atom when a high-electric field is applied [1]. The electron moves from the valence band to the conduction band when the energy applied to the electron is higher than the band-

gap energy [1]. This phenomenon affects an avalanche breakdown, which allows electric current to flow continuously.

Electrons with high energy collide with a bound electron. A pair of free electrons is produced through this process. This pair of free electrons yields two more pairs of free electrons when it gains enough energy from the applied electric field. The density of free electrons increases with repetition in the yields of the free electrons. The increase of free electrons leads to very high local energy loss as a result of local lattice collapse [2].

Avalanche breakdown occurs by a continuous increase of conduction electrons before breakdown. Zener (1934) introduced the theory of field emission critical field strength. Probability per unit time (P_{vc}) that an electron moves from the valence band to the conduction band is calculated by the field emission critical field strength theory [3].

$$P_{vc} = \gamma E^{10/3} \exp\left(-\frac{\beta}{F}\right) \qquad \text{Equation } \mathbf{2.5}$$

$$\beta = 4 \times 10^7 \times \sqrt{\frac{m^*}{m}} \times \sqrt{I}^3 \qquad \text{Equation } \mathbf{2.6}$$

where E is the electric field, F is the critical field strength, m^* is the effective mass at the bottom of the conduction band, and I is the ionization energy. The probability per unit time (P_{vc}) is dependent on the electric field.

The avalanche breakdown mechanism has the characteristic that breakdown strength of a polymer dielectric increases as the thickness of the polymer dielectric in the low-temperature region decreases [4]. Ieda obtained experimental results that can support avalanche breakdown in low-density polyethylene (LDPE) films at liquid nitrogen

temperature [5]. The breakdown strength of the LDPE films increased with decreasing thickness of the films as depicted in Figure **2.4**.

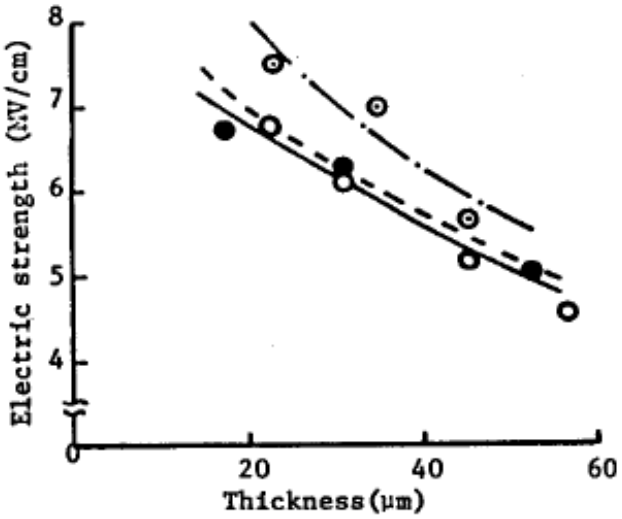

Figure **2.4**: Thickness-dependent DC breakdown strength in LDPE films at -196°C [5]. ○: blank, ⊙: 1wt% pyrene doped, ●: 1wt% AS-1 doped

2.2.2 Thermal Breakdown

Thermal and electrical conductivities in solids are important parameters that govern thermal breakdown. Insulators have a finite resistivity that leads to Joule heating (I^2R). The electrical conductivity increases with temperature, thus increasing Joule heating.

If heat in a material is not removed sufficiently, temperature and electric current rapidly increase until electrical discharge occurs. Materials can be melted and corroded physically and chemically at a certain point with increasing temperature that the thermal conductivity decreases with temperature. Local dielectric breakdown at high temperature

causes global dielectric breakdown resulting in the creation of a conducting channel between electrodes [1]. Heat generation that introduces thermal breakdown is dependent on time, and thus breakdown strength depends on time to breakdown in the applied electric field [1]. For example, Pyrex at 70°C shows 9 MV/cm of breakdown strength when the applied electric field is not continued above 1ms. The breakdown strength, however, is 2.5 MV/cm if the electric field is applied longer than 30 seconds [1]. Thermal breakdown depends on heat transfer, time, and temperature.

Thermal breakdown can be related to destructive breakdown and thermal runaway. First, the mechanical properties of a dielectric material change with temperature. These changes result in a decrease in a material's breakdown strength. This process is called destructive breakdown. Second, an increase of thermal and electrical conductivities, and a dissipation of electrical power in the dielectric material result in an increase of temperature. The increase of temperature causes thermal runaway [2].

The temperature of a polymer dielectric increases by Joule heating resulting from increasing an electric field. The increase of thermal conduction results in an increase of current in the polymer dielectric. Thermal runaway results from the increase in current [6]. The thermal runaway consequently exhibits thermal breakdown, and breakdown strength of the polymer dielectric decreases with increasing temperature [6]. Hikita et al. obtained data showing that polyimide (PI) can support thermal breakdown at 90°C. PI displayed a rise in current before breakdown as a function of time backward from breakdown as shown in Figure **2.5** [6]**.**

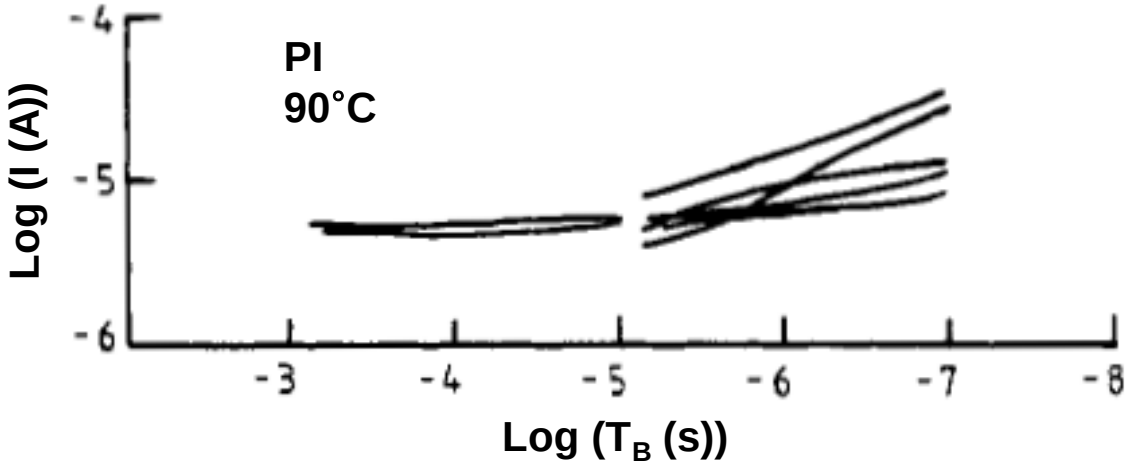

Figure **2.5**: Time backward from breakdown dependence of current before breakdown of PI at 90°C [6]

2.2.3 Electromechanical Breakdown

A dielectric material experiences a compressive stress between electrodes when an electric field is applied because of an electrostatic force resulting from opposite charges of the electrodes as shown in Figure **2.6**. The pressure increases and thickness decreases with increasing applied field. The dielectric material receives more stress with decreasing thickness, and finally, dielectric breakdown will occur. This process can generate heat and increase the temperature of the dielectric material. Heat lowers the mechanical stability of the dielectric material. In addition, the mechanical breakdown occurs when cracks grow under the influence of high stress. In addition, some polymers have poor electromechanical breakdown properties. For such polymers, a decrease in operating temperature is needed to avoid electromechanical breakdown [1].

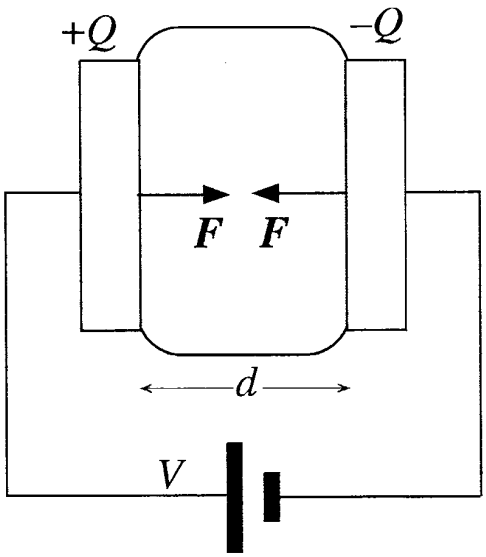

Figure **2.6**: Electrostatic force is induced between electrodes when an electric field is applied to the electrodes [1]

Prior to the electromechanical breakdown of a dielectric material, an equilibrium situation exists in which the dielectric material between electrodes is compressed mechanically. An attractive force (F) is introduced as a function of electrostatic energy. This force is related to the thickness of the dielectric material and applied voltage as displayed in Equation **2.7**.

$$F = \left(\frac{\partial U}{\partial d}\right)_v = \frac{\partial}{\partial d}\left(\frac{1}{2}CV^2\right)_v \qquad \text{Equation } \mathbf{2.7}$$

where U is the energy stored in the system, C is the parallel-plate capacitance of the dielectric material, and V is the constant applied voltage. Next, the electrostatic energy is equated to the mechanical strain energy as given in Equation **2.8**.

$$\frac{\varepsilon_o \varepsilon_r}{2}\left(\frac{V}{d}\right)^2 = Y \ln\left(\frac{d_o}{d}\right) \qquad \text{Equation } \mathbf{2.8}$$

$$V = d\sqrt{\frac{2Y}{\varepsilon_o \varepsilon_r}\ln\left(\frac{d_o}{d}\right)} \qquad \text{Equation } \mathbf{2.9}$$

where ε_o is the permittivity of free pace, ε_r is the relative permittivity, V is the applied voltage, Y is Young's modulus of elasticity, d_o is the initial thickness of the dielectric material, and d is the decreased thickness after applying voltage. The left term of Equation **2.8** is the electrostatic compressive stress, and the right term is the opposing elastic stress [2]. Young's tensile modulus is given in Equation **2.10**.

$$Y = \frac{\Delta\sigma}{\Delta d / d} = \frac{d\Delta\sigma}{\Delta d} \qquad \text{Equation } \mathbf{2.10}$$

where $\Delta\sigma$ is the tensile stress increment, Δd is the increase of sample length, and d is the extended sample length. The stress for a linear elastic material, σ, is expressed by Equation **2.11**.

$$\sigma = \int_{d_o}^{d} \frac{1}{d} dd = \ln\frac{d}{d_o} \qquad \text{Equation } \mathbf{2.11}$$

The instability of mechanical balance is obtained once the thickness in the applied electric field is 60% of initial thickness [3]. Mechanical breakdown occurs when a normalized thickness, d/d_o, is below 0.6 with voltage applied. A critical electric stress (E_c) is given in Equation **2.12**.

$$E_c = \sqrt{\frac{Y}{\varepsilon_o \varepsilon_r}} \qquad \text{Equation } \mathbf{2.12}$$

The highest apparent breakdown strength (E_{Br}) is expressed in Equation **2.13**.

$$E_{Br} = \frac{V_c}{d_o} = \frac{d}{d_o} E_c \approx 0.6\sqrt{\frac{Y}{\varepsilon_o \varepsilon_r}} \qquad \text{Equation } \mathbf{2.13}$$

Stark and Garton (1955) explored this failure mechanism in polyethylene. Young's modulus and breakdown strength in irradiated polyethylene showed a small decrease with increasing temperature when compared with normal polyethylene [7]. The irradiation may be capable of reducing the extent to which breakdown strength decreases with increasing temperature.

The low breakdown strength of rubbery materials is explained by Equation **2.13**. The rubbery materials such as polymers have low Young's modulus resulting in low breakdown strength. Most breakdowns in polymers occur by electromechanical breakdown in the high temperature region [4]. A normalized thickness of the dielectric materials, which is a function of normalized voltage, is depicted in Figure **2.7**.

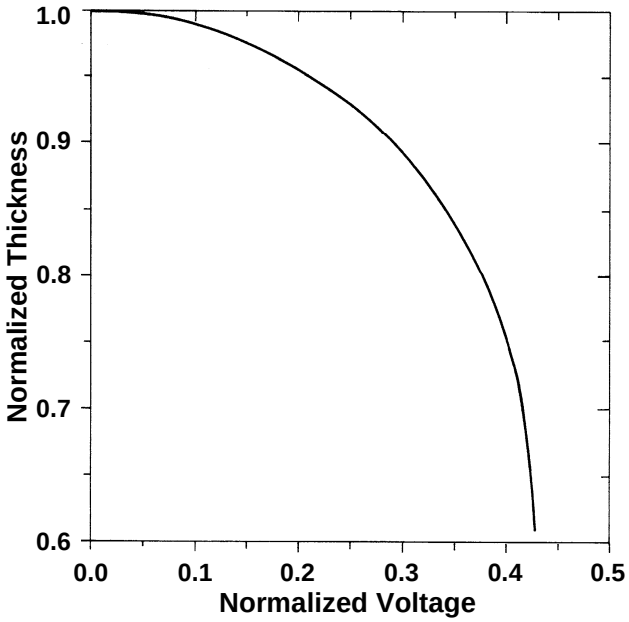

Figure **2.7**: Normalized thickness of a rubbery material as a function of normalized voltage [2]

Electromechanical breakdown is important in polymer dielectrics. The electromechanical breakdown is dominant in the high-temperature region as shown in Figure **2.8** [4]. The breakdown strength of the polymers decreases with increasing temperature. The polymers soften with increasing temperature which is related to the glass transition temperature, T_g. The polymers undergo a transition from a glassy state to a plastic flow state with increasing temperature as displayed in Figure **2.8**. The transition is a function of the molecular motion of polymers. The relaxation modulus also decreases with increasing temperature as depicted in Figure **2.9** [8]. It shows a rapid decrease at T_g. The decrease of the breakdown strength in the polymers at a high temperature can be related to an instability of mechanical balance [3]. Stark and Garton considered this decrease of breakdown strength to be related to the electromechanical breakdown [3]. They showed that the mechanical strength of polymer dielectrics changed at a higher temperature. An abnormal decrease of breakdown strength in the polymers above T_g is shown at T_{c2} as expressed in Figure **2.8**. T_{c2} may be related to the melting temperature of the polymers. The relaxation modulus of polystyrene (PS) decreases again with increasing temperature above a rubbery flow region as displayed in Figure **2.9**. The decrease of the relaxation modulus is continued with the approaching melting temperature (~513K) of PS [9]. The decrease in the relaxation modulus may result in the decrease of breakdown strength with increasing temperature above T_{c2}.

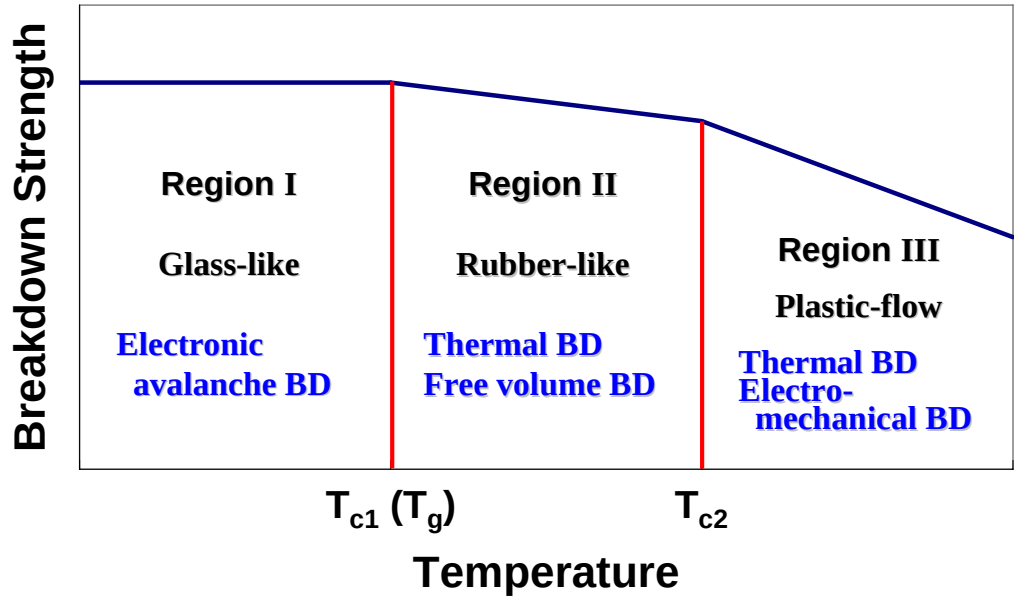

Figure **2.8**: Outline of the temperature dependence of breakdown strength in linear polymers [4]

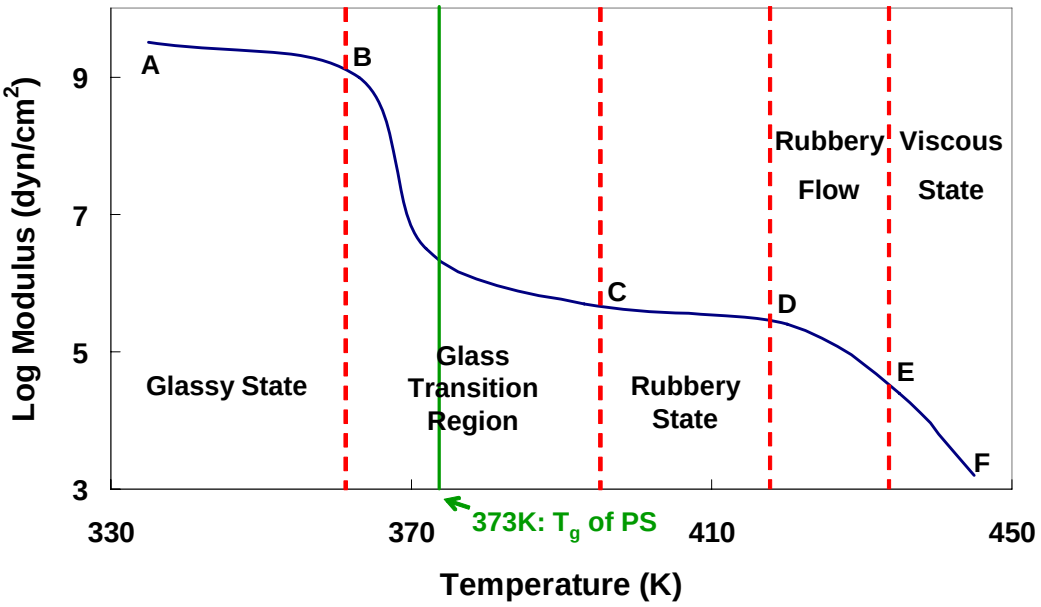

Figure **2.9**: Five regions of viscoelasticity depending on temperature for polystyrene (PS). Relaxation modulus of PS varies with temperature [8]

2.3 Structure of Polymer Dielectrics

Polymers have different glass-transition temperatures (T_g) and degrees of crystallinity. Studying these properties will be useful for understanding the thermal and structural behaviors of the polymer dielectrics. General concepts regarding T_g and crystallinity are introduced in this section. The breakdown strength of polymer dielectrics as related to temperature, polarity, and cohesive-energy density are introduced.

2.3.1 Glass-transition Temperature

The glass-transition temperature (T_g) is an important factor to consider in starting an investigation of a new material. Polymers undergo a transition from the glassy state to the rubbery state with increasing temperature as shown in Figure **2.9**. This transition affects the properties of polymers. The transition is a function of the molecular motion of polymers. Polymer chains move easily in the rubbery state. However, the movement decreases with decreasing temperature because of insufficient thermal energy, which can get over the rotational energy barriers in polymer chains [8]. At the glass-transition temperature, the movement of polymer chains almost ceases. The relaxation modulus increases rapidly with decreasing temperature [8].

The glass transition occurs in amorphous (or glassy) and semi-crystalline polymers generally [10]. However, amorphous polymers exhibit this behavior to a greater extent than do semi-crystalline polymers. T_g is difficult to determine in highly crystalline polymers [11]. The motion of molecular chains decreases with decreasing temperature. Stiffness, heat capacity, and the coefficient of the thermal expansion of the polymers

change during the glass transition [10]. Differential scanning calorimetry (DSC) and thermo mechanical analysis (TMA) are generally used to measure T_g.

2.3.2 Crystallinity

The extent of the crystallinity of polymers is determined by the degree to which the molecular order is arranged by a packing of polymer chains, that is, the tighter the arrangement of the polymer chains the greater the crystallinity. Polymer molecules twist when molten because the polymer chains are flexible in that state. The polymer chains become rigid with decreasing temperature due to the rearrangement of polymer molecules with decreasing free volume. Crystallization of the polymers occurs if the cooling time of the polymer molecules is long enough to rearrange the polymer molecules [7]. However, amorphous states are introduced if the cooling time for rearranging the polymer molecules is not long enough for this purpose. Partially crystalline states will occur through this process. No polymers have 100% crystallinity. The degree of crystallinity of most polymers ranges from 5% to 50% [7]. The crystallization occurs above T_g because lower temperatures do not produce sufficient chain movements [7]. The degree of crystallinity is ascertained by using specific volume in the polymers. X-ray diffraction is also used to measure the degree of crystallinity by comparing the area under crystalline and amorphous peaks. The degree of crystallinity affects the mechanical properties of polymers. Broad secondary bonds are between chain segments in the crystalline region [12]. The secondary bonds are much less dominant in the amorphous region than in the crystalline region [12].

2.3.3 Cohesive Energy Density related to Dielectric Breakdown in Polymers

There is a correlation between breakdown strength and cohesive-energy density (CED) in polymers. The cohesive-energy density is expressed by Equation **2.14**. The cohesive-energy density indicates the binding force between molecular chains in the polymers [2].

$$CED = \frac{\Delta H_{vap} - RT}{\overline{V}} \qquad \text{Equation } \mathbf{2.14}$$

where ΔH_{vap} is the heat of vaporization, R is the gas constant, T is temperature, and $\overline{V}$ is the molar volume. Polar polymers show higher breakdown strength and cohesive-energy density than non-polar polymers in Figure **2.10** because the polar polymers have strong polar side groups, which induce a higher dipole moment than do the non-polar polymers.

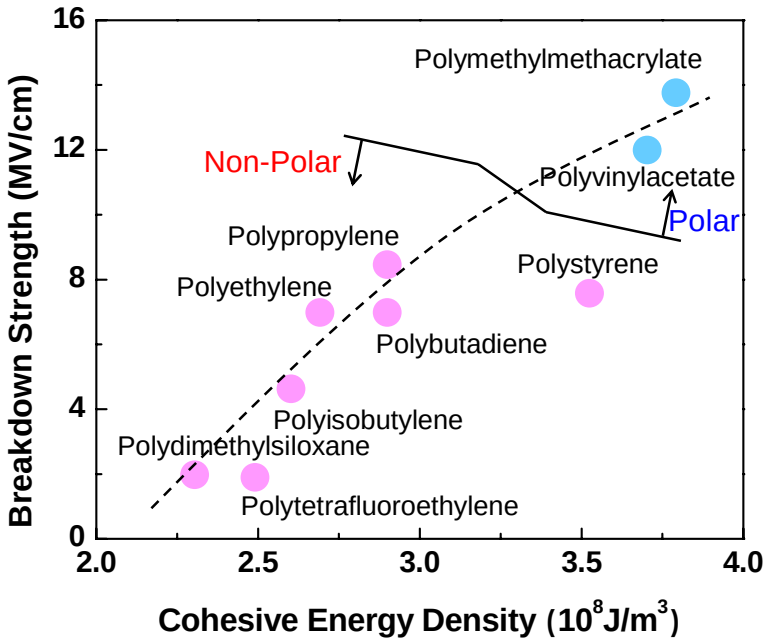

Figure **2.10**: Correlation between breakdown strength and cohesive energy-density in polar/non-polar polymers [2, 13, 14]

Correlation between the cohesive-energy density and breakdown strength for low-density polyethylene (LDPE) with temperature is displayed in Figure **2.11**. The cohesive-energy density of LDPE increased with decreasing temperature [2]. The breakdown strength of LDPE also showed an increase with decreasing temperature as discussed in regard to the breakdown behavior of polymer dielectrics in Chapter **1** [2]. This behavior indicates that the increase of breakdown strength with decreasing temperature in polymer dielectrics can be related to cohesive-energy density.

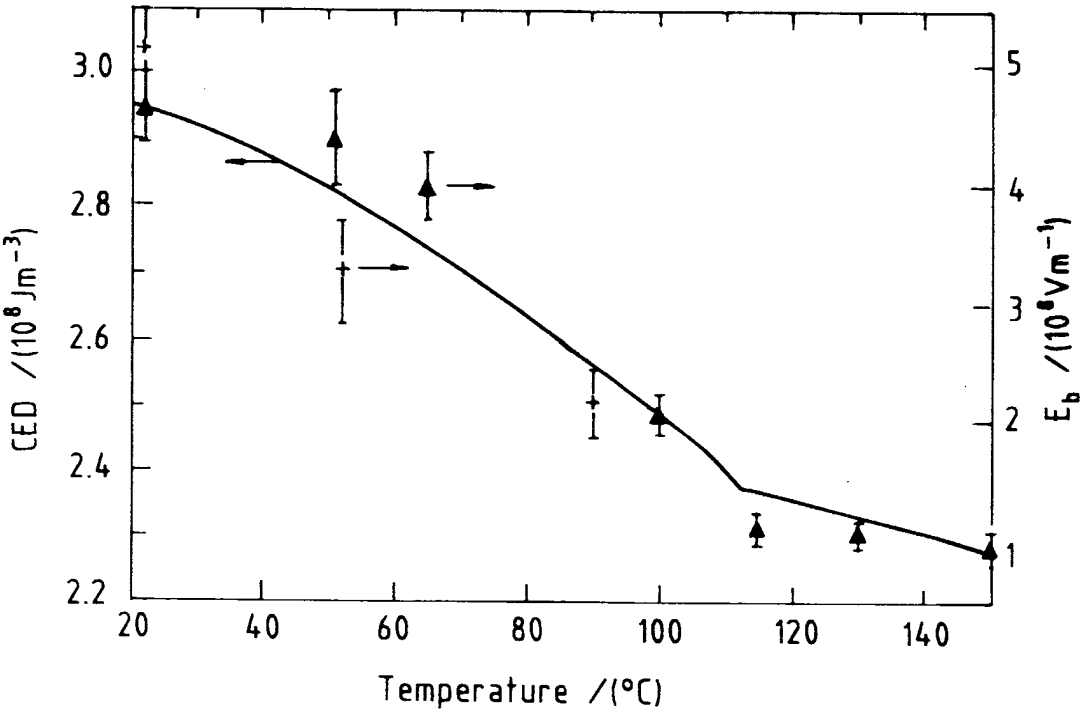

Figure **2.11**: Correlation between breakdown strength (E_b) and cohesive-energy density (CED) with changing temperature for low-density polyethylene (LDPE). The solid line indicates the cohesive-energy density, and the symbols define the breakdown strength [2]

In the next chapter, an experimental approach for investigating electrical properties in polymer dielectrics including polypropylene (PP), polyimide (PI), polymethyl methacrylate (PMMA), poly(vinylidene fluoride-trifluoroethylene-

chlorotrifluoroethylene) terpolymer (p(VDF-TrFE-CTFE)) will be introduced. The general properties of the polymers are presented. An experimental procedure for low-field permittivity (ε_r) and dielectric loss ($\tan\delta$) at room temperature and as a function of temperature is expressed. An experimental procedure for dielectric-displacement measurements to calculate high-field permittivity is also introduced. Dielectric breakdown measurements and mechanisms for maintaining temperature will be presented.

References

1. S.O. Kasap, Principles of Electronic Materials and Devices, 3rd ed, McGraw-Hill (2005)
2. L.A. Dissado, J.C. Fothergill, Electrical Degradation and Breakdown in Polymers, London, Peter Peregrinus Ltd. (1992)
3. E. Furman, Dielectric Breakdown and Related Properties of Lead Lanthanum Zirconate Titanate 9.5/65/35, The Pennsylvania State University (1987)
4. M. Ieda, M. Nagao, and M. Hikita, High-field Conduction and Breakdown in Insulating Polymers, IEEE Transactions on Dielectrics and Electrical Insulation, 1, 934-945 (1994)
5. M. Ieda, Dielectric Breakdown of Polyethylene Films at Cryogenic Temperature, Science Contributions, 2, (1-05), 414-420 (1979)
6. M. Hikita, Investigation of electrical breakdown of polymeric insulating materials using a technique of pre-breakdown current measurements, in Journal of physics. F, Metal physics, 1515 (1990)
7. T. Blythe, D. Bloor, Electrical Properties of Polymers, 2nd ed, New York, Cambridge University Press (2005)
8. J.M.G. Cowie, Polymers: Chemistry & Physics of Modern Materials, 2nd ed, New York, Blackie (1991)
9. J. Brandrup, E.H. Immergut, Polymer Handbook, 3rd ed, New York, Wiley (1989)
10. R.J. Young, P.A. Lovell, Introduction to Polymers, 2nd ed, London, Chapman & Hall (1991)
11. F.W. Billmeyer, Textbook of Polymer Science, 3rd ed, New York, John Wiley & Sons (1984)
12. R.B. Richards, Polyethylene-Structure, Crystallinity and Properties, Journal of applied chemistry, 1, (8), 370-376 (1951)
13. J.-P. Crine, A.K. Vijh, Influence of the cohesive energy density of polymers and of the nature of metal-polymer interface on the contact charging of polymers, Proceedings of the Electrical Insulation and Dielectric Phenomena, 1989. Annual Report., Conference on, 284-289 (1989)
14. G. Raju, A. Katebian, and S.Z. Jafri, Application of Weibull distribution for high temperature breakdown data, Proceedings of the Electrical Insulation and Dielectric Phenomena, 2001 Annual Report. Conference on, 173-176 (2001)

Chapter 3

Experimental Approach

3.1 Introduction

The following polymers including polypropylene (PP), polyimide (PI), polymethyl methacrylate (PMMA), and poly(vinylidene fluoride-trifluoroethylene-chlorotrifluoroethylene) terpolymer (p(VDF-TrFE-CTFE) terpolymer) were used in this study. The general properties of the polymers and experimental procedures for investigating the electrical properties of the polymers will be introduced in this chapter. The properties of the various polymers are summarized in Table **3.1**. PP shows the highest degree of crystallinity (40%–65%) with a relatively high melting temperature (T_m=~165°C), breakdown strength (~6.4MV/cm), and relatively low glass-transition temperature
(T_g=-17°C – -10°C). Electrically, PP possesses the lowest relative permittivity (ε_r=2.2–2.3) and dielectric loss (tanδ<0.5%) at 1kHz. PI shows the highest T_g (260°C–270°C) and T_m (350°C–400°C) with a relatively low degree of crystallinity (35%–50%). PI exhibited a relatively low ε_r (~2.8) dielectric loss (<0.5%) at 1kHz, and breakdown strength (~4.0MV/cm). PMMA displayed the highest breakdown strength (~10MV/cm) with a relatively high T_g (~105°C), relatively high degree of crystallinity (25%–60%), and relatively high dielectric loss (~5.5%). It also showed a relatively low T_m (130°C–

140°C) and ε_r (~3.0). P(VDF-TrFE-CTFE) terpolymer exhibited the highest ε_r (~50) and the highest dielectric loss (~10%) due to its higher dipole moment. The terpolymer displayed a relatively low T_m (40°C−160°C) with the lowest T_g (-20°C – -10°C), lowest degree of crystallinity (15%–50%), and lowest breakdown strength (1.0–3.5MV/cm). The properties of the terpolymer varied with various compositions.

Table **3.1**: General properties of various polymers including PP, PMMA, PI, and p(VDF-TrFE-CTFE) terpolymer [1-16]

Polymer	T_g (°C)	T_m (°C)	Tensile Strength (MPa)
Polypropylene	-17 – -10 [6]	~165 [6]	29–39 [6]
Polyimide	260–270 [17]	350–400 [18]	~230 [1]
Polymethyl methacrylate	~105 [6]	130–140 [6]	~80 [6]
P(VDF-TrFE-CTFE) terpolymer	-20 – -10 [4]	40–160 [4]	~400 [2]

Polymer	Crystallinity (%)	Relative Permittivity (ε_r at 1kHz)	Dielectric Loss (tanδ at 1kHz, %)
Polypropylene	40–65 [6, 12]	2.2–2.3 [6]	<0.5 [16]
Polyimide	35–50 [7, 9]	~2.8 [19]	<0.5 [11]
Polymethyl methacrylate	25–60 [6]	~3.0 [6]	~5.5 [6]
P(VDF-TrFE-CTFE) terpolymer	15–50 [13]	~50 [5]	~10 [4]

Polymer	Breakdown Strength (MV/cm)	Molecular Weight (M_w X 10^{-5} g/mol)	Polarity
Polypropylene	~6.4 [20]	1.5–3 [6]	Non-polar
Polyimide	~4.0 [21]	1–5 [14]	Non-Polar
Polymethyl methacrylate	~10 [8]	5–20 [10]	Polar
P(VDF-TrFE-CTFE) terpolymer	1.0–3.5 [15]	0.5–2 [13]	Polar

In this chapter, the material selection, film preparation, and experimental procedure for electrical property measurements including temperature dependence for breakdown will be discussed.

3.2 Materials

3.2.1 Polypropylene (PP)

Thin film polypropylene is commonly used as a dielectric for capacitors. PP shows high performance for pulsed power with low dielectric loss, high insulation resistance, and long-term stability [22]. There are three kinds of polypropylene including isotactic, atactic, and syndiotactic as introduced in **3.3.1.4**. The melting temperature is around 165°C, which is relatively high for polymers as shown in Table **3.1** [6]. The glass-transition temperature ranges from -17°C to -10°C [6]. The isotactic PP has higher crystallinity (40%–65%), breakdown strength (~6.4MV/cm) than other polymers as shown in Table **3.1** [6]. Isotactic PP shows low dielectric loss (tanδ) at below 0.5% at 1kHz [6]. The monomer of PP is compounded with 2 carbons, 3 hydrogens, and 1 methyl group as depicted in Figure **3.1**. Orientations of the methyl groups in PP chains define tacticity. PP is a non-polar polymer. The methyl groups in PP induce a low dipole moment in molecules, resulting in a low relative permittivity (ε_r=2.2–2.3 at 1kHz).

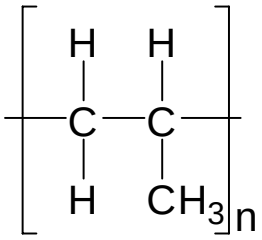

Figure **3.1**: Chemical structure of PP. A methyl group is bonded with a carbon of a propylene monomer. The orientation of the methyl groups defines tacticity in PP

3.2.2 Polyimide (PI)

Polyimide shows high-tensile strength and thermal stability as listed in Table **3.1**. Polyimide possesses high T_ms (350°C –400°C) and T_gs (260°C –270°C), slightly higher than other polymers [6]. Polyimide can be used for applications that require a high operating temperature due to its high melting temperature. It exhibits a relatively lower degree of crystallinity (35%–50%), and breakdown strength (~4.0MV/cm) [1, 7, 9]. The chemical structure of polyimide is derived from polyamic acid (PAA) [23]. Phenyl groups in PI induce a relatively high dipole moment in the molecule. The relatively high dipole moment results in a large relative permittivity of PI.

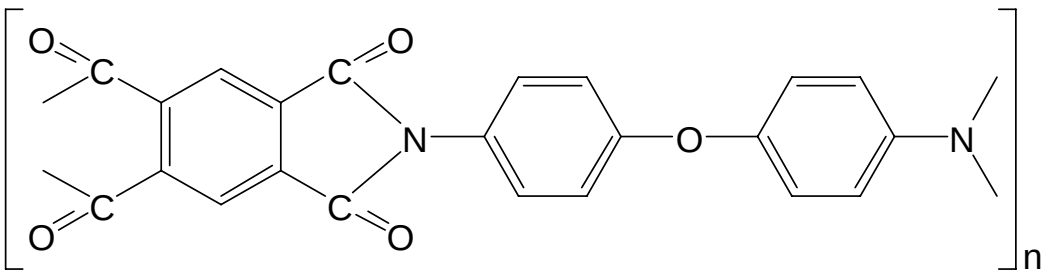

Figure **3.2**: Chemical structure of polyimide (PI). The chemical structure of the polyimide is derived from polyamic acid [23]

3.2.3 Polymethyl Methacrylate (PMMA)

Polymethyl methacrylate (PMMA) displays high heat resistance, rigidity, and chemical resistance [22]. PMMA is used for an alternate glass because of high transparency and impact strength. In the TFT-LCD (thin film transistor-liquid crystal display) industry, PMMA is used as a light guide for backlights. The glass-transition temperature of PMMA is around 105°C and its melting temperature is 130°C –140°C [6]. PMMA shows relatively higher crystallinity (25%–60%) than other polymers as shown in Table **3.1** [6, 8, 10]. It also exhibits the highest breakdown strength (~10MV/cm). The dielectric loss of PMMA is slightly higher (~5.5% at 1kHz) than that of other polymers except the p(VDF-TrFE-CTFE) terpolymer [6]. An MMA monomer contains a methyl and a methacrylic group. P(VDF-TrFE-CTFE) terpolymer is a polar polymer. The orientation of these groups defines the tacticity of PMMA chains as shown in **3.2.1.3**. PMMA is a polar polymer. Methacrylate groups in PMMA induce a relatively high dipole moment in the molecule. The relatively high dipole moment results in a higher relative permittivity for PMMA than that for PP.

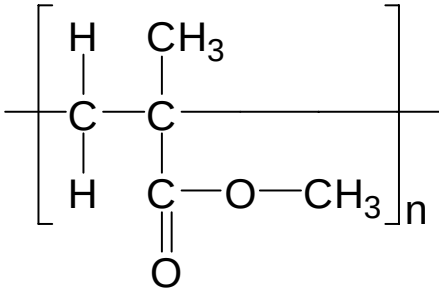

Figure **3.3**: Chemical structure of polymethyl methacrylate (PMMA). A monomer of PMMA contains a methyl and a methacrylic group. The tacticity of PMMA chains is defined by the orientation of the groups

3.2.4 P(VDF-TrFE-CTFE) Terpolymer

Poly(vinylidene fluoride-trifluoroethylene-chlorotrifluoroethylene) terpolymer is an example of a ferroelectric polymer. The terpolymer was polymerized from the poly(vinylidene fluoride-trifluoroethylene) copolymer, which is a semi-crystalline polymer. The copolymer shows strong polarization originating from the spontaneous orientation of dipoles [5]. Chlorotrifluoroethylene (CTFE) was added to the copolymer as depicted in Figure **3.4**. This terpolymer shows high relative permittivity (50 at 1kHz), significantly higher than other polymers [3]. However, its dielectric loss is also very high (10% at 1kHz) [3]. The high dielectric loss influences the relatively low breakdown strength in terpolymer (1.0–3.5MV/cm) [15]. The dielectric properties are strongly dependent on the change of the chemical composition in the terpolymer [5]. The terpolymer also displays strong frequency dependence of relative permittivity and dielectric loss—this is typical of relaxor ferroelectrics [3]. The degree of crystallinity (15%–50%), T_g (-20°C – -10°C), and T_m (40°C –160°C) of the terpolymer can be varied by changing the chemical composition in the terpolymer as presented in Table **3.1** [4, 5]. The chemical composition of the terpolymer was 78.8/7.2/14.0 (VDF/TrFE/CTFE) mol% [24]. Fluorine and chlorine atoms induce a high dipole moment in the molecule [25].

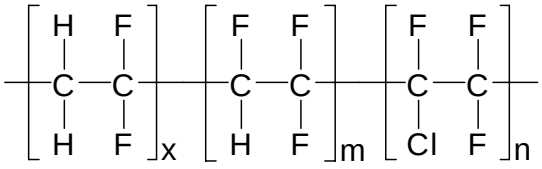

Figure **3.4**: Chemical structure of p(VDF-TrFE-CTFE) terpolymer. CTFE is introduced into the p(VDF-TrFE) copolymer. Properties of the terpolymer vary with changing chemical composition

The chemical composition of the p(VDF-TrFE-CTFE) terpolymer influences breakdown strength. Claude et al. reported the TrFE concentration dependence of the terpolymer's breakdown strength as depicted in Figure **3.5** [15]. The breakdown strength increased as the concentration of TrFE increased. The increase of the breakdown strength was due to an increase of the degree of crystallinity as listed in Table **3.2**, which gives resistivity to electromechanical breakdown in polymers [15].

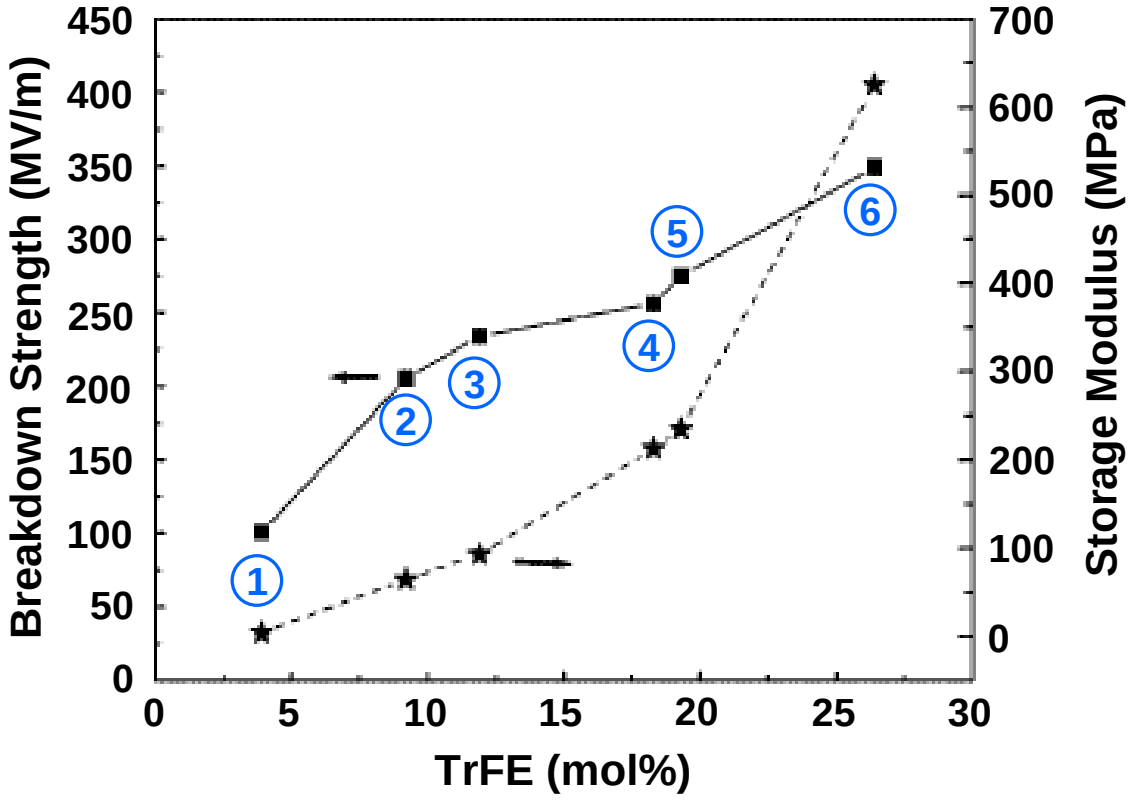

Figure **3.5**: TrFE concentration dependence of breakdown strength and storage modulus for p(VDF-TrFE-CTFE) terpolymer [15]

Table **3.2**: Various compositions and degrees of crystallinity for p(VDF-TrFE-CTFE) terpolymer [15]

	Composition (mol%)			
Polymer	VDF	TrFE	CTFE	Degree of Crystallinity (%)
1	73.6	3.9	22.5	14.4
2	73.6	9.2	17.2	17.1
3	73.6	11.9	14.5	18.0
4	73.6	18.3	8.1	24.2
5	73.6	19.3	7.1	28.6
6	73.6	26.4	0	35.4

3.3 Film Preparation

Several polymer films, presented above, were prepared so that their electrical properties could be investigated. The thicknesses and drawings for the various polymer films are summarized in Table **3.3**. Only bottom electrodes were used for breakdown measurements as depicted in Figure **3.6** (a). Top and bottom electrodes were used to determine the relative permittivity, dielectric loss, and dielectric displacement measurements as shown in Figure **3.6** (b). Circular electrodes 10mm in diameter were deposited on top of the films for the measurements. The thickness of the electrodes was 50nm.

Table **3.3**: Thickness and electrode material for the various polymer films. The thickness of electrodes was about 50nm

Polymer	Thickness (μm)	Drawing	Source
Polypropylene	12	Yes (biaxially)	Electronic Concepts, Inc.
Polyimide	13	No	Goodfellow Corporation
Polymethyl methacrylate	20	Yes (from 50μm, monoaxially)	Goodfellow Corporation
P(VDF-TrFE-CTFE) terpolymer	20	No	Piezotech

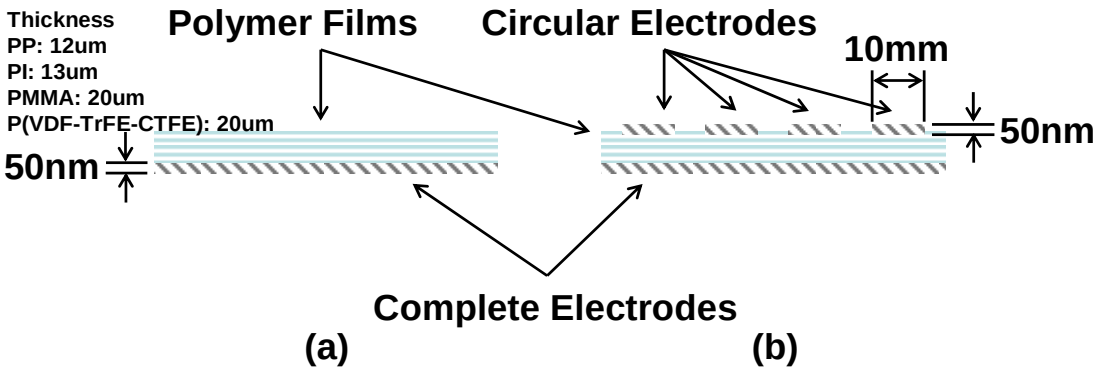

Figure **3.6**: Electrode configurations for measurements of electrical properties including (a) breakdown (b) relative permittivity, dielectric loss, and dielectric displacement

3.3.1 Polymer Films

As listed in Table **3.3**, metalized 12μm thick isotactic PP films (Electronic Concepts, P.O. Box 1278, Eatontown, NJ 07724, USA) were used to investigate electrical properties. The PP films were biaxially stretched with one side of the film covered with an aluminum layer.

Kapton® Type HN polyimide films (Goodfellow Corporation, 305 High Tech Drive, Oakdale, PA 15071, USA) were used in this study. The thickness of the films was 13 μm.

As received PMMA films (Goodfellow Corporation, 305 High Tech Drive, Oakdale, PA 15071, USA) were 50μm thick. The films were monoaxially stretched to about 20μm thick by using a zone-drawing machine.

The thickness of the p(VDF-TrFE-CTFE) terpolymer films was 20μm. The films were synthesized at Piezotech (F. Bauer, PIEZOTECH S.A., 9 rue de Colmar, 68220 Hesingue, France). TRS Technologies (Edward F. Alberta, TRS Technologies, 2820 East College Avenue, Suit J, State College, PA 16801, USA) produced the terpolymer films through a solution casting method.

3.4 Relative Permittivity and Dielectric-Loss Measurements

Relative permittivity and dielectric loss were investigated by impedance spectroscopy. A small AC voltage (~1V) was applied to the samples. The temperature dependence of relative permittivity and dielectric loss were determined from -184°C to 180°C. Data were measured at different frequencies (1kHz, 10kHz, and 100kHz). A HP 4284A precision LCR meter and a HP 3478A digital multi-meter (Agilent Technologies, Inc., 5301 Stevens Creek Blvd., Santa Clara, CA 95051) were used to calculate relative permittivity and dielectric loss from the capacitance measurements. The temperature dependence of relative permittivity and dielectric loss were also investigated in this study.

Temperature was controlled by using a Delta design 9023 environmental test chamber (Delta Design, Inc., 12367 Crosthwaite Circle Poway, CA 92064). The experimental setup for relative permittivity and dielectric-loss measurements is depicted in Figure **3.8**.

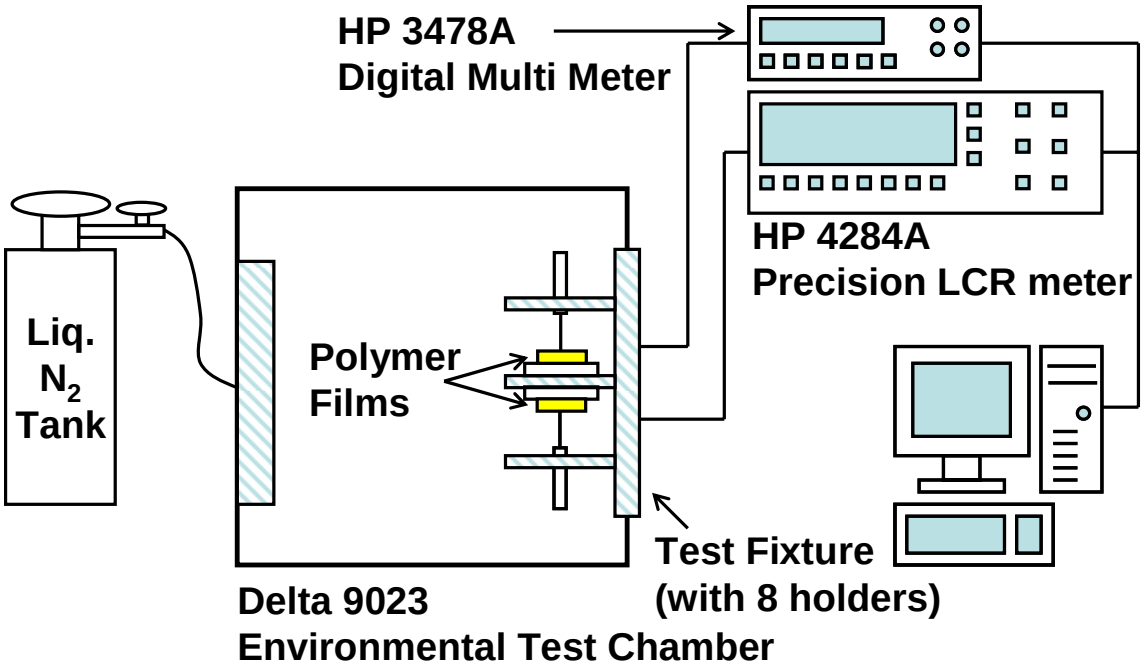

Figure **3.7**: Experimental setup for relative permittivity and dielectric-loss measurements [26]

3.5 Dielectric-Displacement Measurements

The experimental setup for dielectric-displacement measurements is shown in Figure **3.8**. A mushroom holder was used for dielectric displacement (polarization) measurements. It had a 5mm rounded copper dome used as the bottom electrode as depicted in Figure **3.10**. An electric field of 1.5MV/cm−6.5MV/cm was applied to the various polymer films.

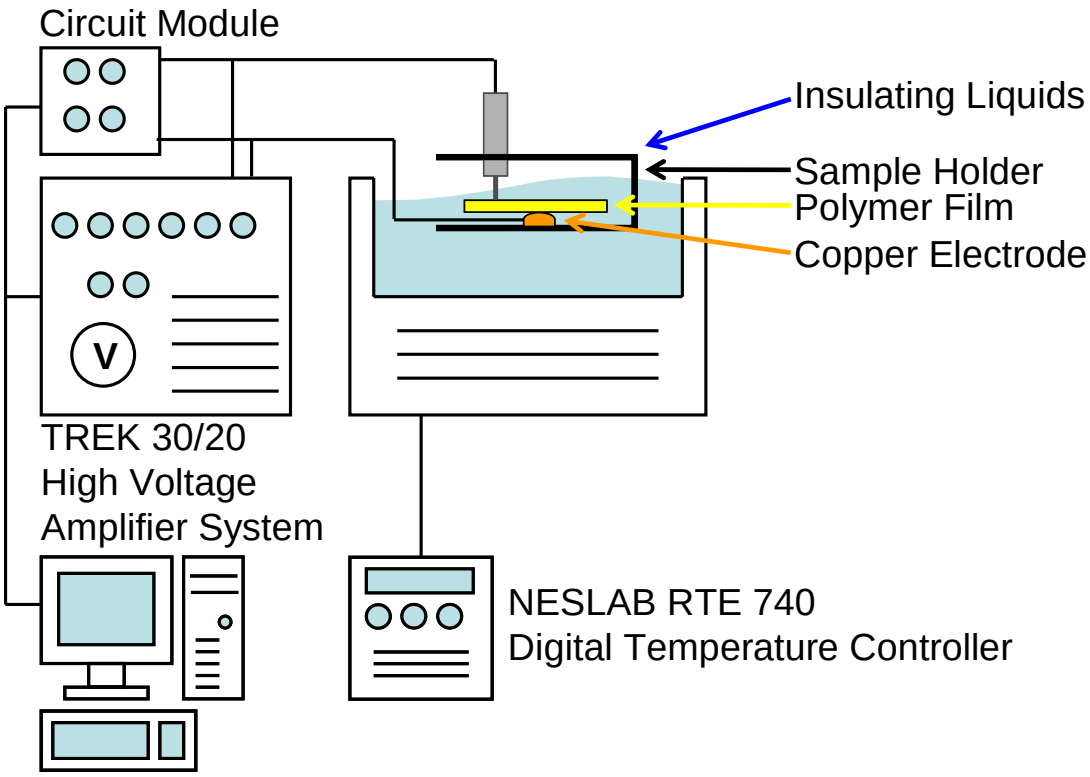

Figure **3.8**: Experimental setup for dielectric-displacement and -breakdown measurements. Temperatures were maintained for the breakdown measurements [27]

A modified Sawyer-Tower circuit was used to measure the dielectric displacement, high-field permittivity, and dielectric loss [27, 28]. Charge (Q) was calculated by measuring voltages across a dielectric (Q=CV). If the circuit is used for a normal dielectric, a linear response will be shown [29]. The polarization is directly related to the applied electric field ($P=\varepsilon_o\varepsilon_r E$). The equations and the plot related to the dielectric displacement were introduced in Chapter **1**. For ferroelectric materials, polarization remained with an electric field [29]. The modified Sawyer-Tower circuit is depicted in Figure **3.9**.

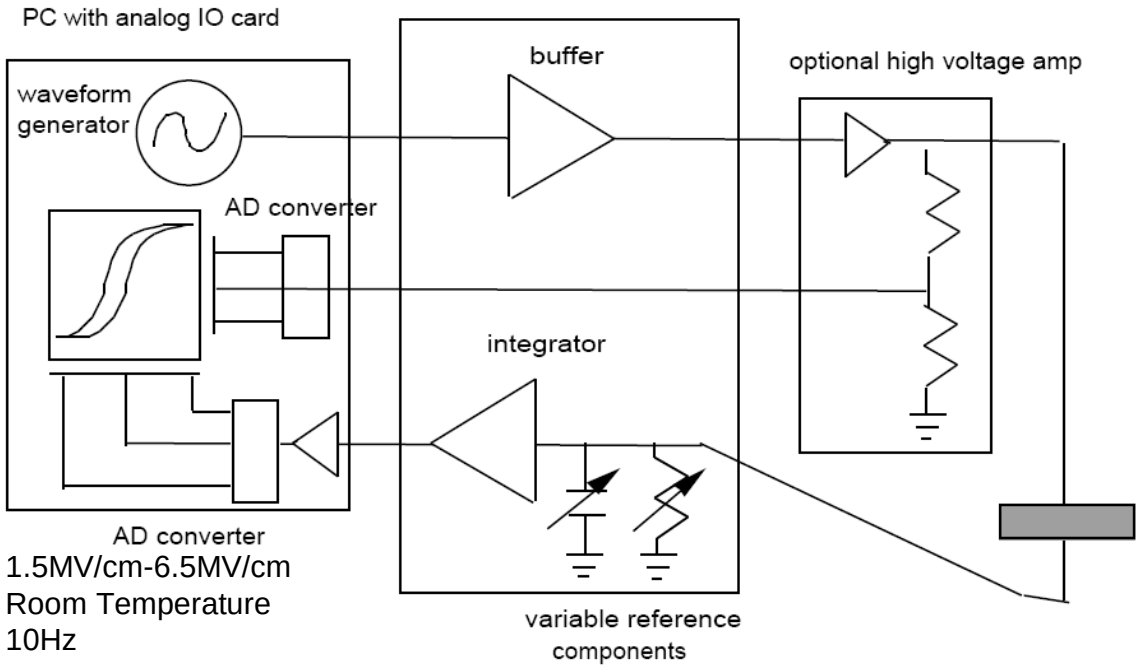

Figure **3.9**: Modified Sawyer-Tower circuit at 1.5MV/cm–6.5MV/cm, 10Hz, and room temperature. In P-E, a linear dielectric shows a linear response, and a ferroelectric material exhibits a non-linear response [27, 29]

3.6 Breakdown Measurements

The experimental setup for the breakdown measurements is given in Figure **3.8**. Galden® heat-transfer fluids were used as an insulating liquid for breakdown measurements at room temperature. Various insulating liquids were also used to maintain temperature during breakdown measurements with temperatures as listed in Table **3.4**. A NESLAB RTE 740 digital temperature controller and liquid bath (Thermo Fisher Scientific, Inc., 81 Wyman Street, Waltham, MA 02454), which included the heat transfer fluid, was used to control temperature from -40°C to 170°C. The temperature

controller was capable of controlling temperatures from -40°C to 200°C. The temperature stability of the controller was ±0.01°C.

A Dewar vacuum bottle, cooling agents, and selected organic liquids were used to decrease the temperature to below -40°C. The Dewar vacuum bottle was used to maintain the low temperatures. Liquid nitrogen and dry ice were used as the cooling agents. The organic liquids such as n-heptane, n-hexane, and n-pentane, as well as liquid nitrogen were used. The decrease of temperature was controlled by the boiling point of liquid nitrogen, the melting point of the organic liquids, and the sublimation point of dry ice. Controlled temperature regions are summarized in Table **3.4**.

Table **3.4**: Insulating media for the investigation of temperature dependence of dielectric breakdown in various polymer films. (BP: boiling point, MP: melting point, SP: sublimation point) [30–32]

Temperature (°C)	Insulating Media	Cooling Agent	Maintaining Temp.
-196	Liquid N_2	Liquid N_2	BP of Liquid N_2
-150	iso-Pentane	Liquid N_2	MP of iso-Pentane
-123	n-Pentane	Liquid N_2	MP of n-Pentane
-98	n-Hexane	Liquid N_2	MP of n-Hexane
-65	n-Heptane	Dry Ice	SP of Dry Ice
-40–170	Galden® HT	-	Refrigerant (SUVA® 404A)

There were two sample holders in breakdown strength measurements as depicted in Figure **3.10**. These holders were used to compare the holder shape effect on breakdown strength. One holder was called a trough holder. It had a flat copper electrode and a plastic spacer to separate the copper electrode on the holder from the polymer film. The second holder was called a mushroom holder. It used a 5mm rounded copper dome as the bottom electrode. Metallic electrodes, positioned on each side of the polymer films,

were used as the top electrodes. Electrostatic attraction between the films and the bottom electrode on the holders occurred at ~0.1MV/cm field (200–500V). High voltages (up to 30kV) were applied by a power supply, TREK 30/20 high-voltage amplifier system (TREK Inc., 11601 Maple Ridge Road, Medina, NY 14103). A ramp rate of 500V/s was used for all breakdown measurements. A high-electric field at 500V/s of ramp rate was applied to the polymer films until breakdown occurred. All breakdown measurements were performed 20 times at each temperature in order to obtain reliable data with Weibull statistics.

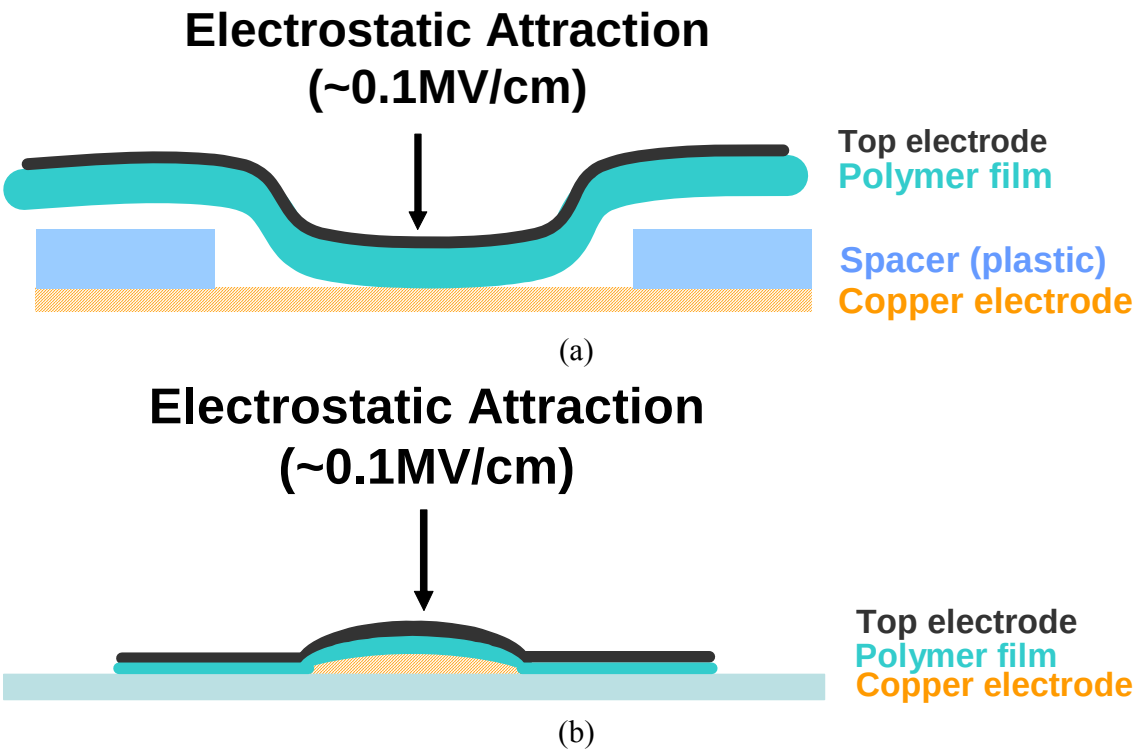

Figure **3.10**: Two sample holders including (a) trough holder and (b) mushroom holder used for breakdown-strength measurements

In the next chapter, the electrical properties of the various polymer films will be discussed. Low-field permittivity and dielectric loss at room temperature and temperature dependence of the permittivity and loss were studied. High-field permittivity at room temperature was calculated from the dielectric displacement. The breakdown strength of the polymer films was measured at room temperature, and the data were analyzed using Weibull distribution. The temperature dependence of dielectric breakdown in the polymer films will be also discussed.

References

1. Good Fellow, Technical Data – Material Properties, http://www.goodfellow.com/csp/active/gfHome.csp, (2008)
2. C. Huang, Q. Zhang, Enhanced Dielectric and Electromechanical Responses in High Dielectric Constant All-Polymer Percolative Composites, Advanced Functional Materials, 14, (5), 501–506 (2004)
3. B. Chu, X. Zhou, B. Neese, Q.M.A.-Z. Zhang, Q.M., and F.A.-B. Bauer, F., Relaxor ferroelectric poly(vinylidene fluoride-trifluoroethylene-chlorofluoroethylene) terpolymer for high energy density storage capacitors, Dielectrics and Electrical Insulation, IEEE Transactions on [see also Electrical Insulation, IEEE Transactions on], 13, (5), 1162–1169 (2006)
4. Y. Lu, J. Claude, B. Neese, Q. Zhang, and Q. Wang, Supporting Information-A Modular Approach to Ferroelectric Polymers with Chemically Tunable Curie Temperatures and Dielectric Constants, The Pennsylvania State University (2006)
5. Y. Lu, J. Claude, B. Neese, Q. Zhang, and Q. Wang, A Modular Approach to Ferroelectric Polymers with Chemically Tunable Curie Temperatures and Dielectric Constants, J. Am. Chem. Soc., 128, (25), 8120–8121 (2006)
6. J. Brandrup, E.H. Immergut, Polymer Handbook, 3rd ed, New York, Wiley (1989)
7. C. Koning, Enhancement of the crystallinity of a thermoplastic polyimide, in Polymer, 5619–5625 (1996)
8. M. Ieda, M. Nagao, and M. Hikita, High-field Conduction and Breakdown in Insulating Polymers, IEEE Transactions on Dielectrics and Electrical Insulation, 1, 934–945 (1994)
9. C.E. Koning, L. Teuwen, A. De Plaen, and J.P. Mercier, Enhancement of the crystallinity of a thermoplastic polyimide, Polymer, 37, (25), 5619–5625 (1996)
10. K. Fukao, Dynamics in thin polymer films by dielectric spectroscopy, The European Physical Journal E – Soft Matter, 12, (1), 119–125 (2003)
11. G. Xu, C.C. Gryte, A.S. Nowick, S.Z. Li, Y.S. Pak, and S.G. Greenbaum, Dielectric relaxation and deuteron NMR of water in polyimide films, Journal of Applied Physics, 66, (11), 5290–5296 (1989)
12. A. Nogales, B.S. Hsiao, R.H. Somani, S. Srinivas, A.H. Tsou, F.J. Balta-Calleja, and T.A. Ezquerra, Shear-induced crystallization of isotactic polypropylene with different molecular weight distributions: in situ small- and wide-angle X-ray scattering studies, Polymer, 42, (12), 5247–5256 (2001)
13. M.T. Chung, Semicrystalline Ferroelectric Fluoropolymers and Process for Preparing Same, United States Patent 6355749, (2002)
14. M. Mikawa, S. Nagaoka, and H. Kawakami, Gas permeation stability of asymmetric polyimide membrane with thin skin layer: effect of molecular weight of polyimide, Journal of Membrane Science, 208, (1–2), 405–414 (2002)
15. J. Claude, Y. Lu, K. Li, and W. Wang, Electrical Storage in Poly(vinylidene fluoride) based Ferroelectric Polymers: Correlating Polymer Structure to Electrical Breakdown Strength, American Chemical Society, 20, (6), 2078–2080 (2008)

16. J. Strydom, Dielectric Measurements for Power Electronic Applications, in IEEE transactions on industry applications, 829 (2001)
17. Everett Charles Technologies, Typical Tg Ratings for the More Common Material Systems, http://www.ectinfo.com/files/resource/technical/esh27.htm, (2003)
18. A. Mian, G. Newaz, T. Mahmood, and G. Auner, Mechanical Characterization of Glass/Polyimide Microjoints Fabricated using CW Fiber and Diode Lasers, Journal of Materials Science, 42, 8150–8157 (2007)
19. Clipper Controls, Dielectric Constant Reference Guide, http://www.clippercontrols.com/info/dielectric_constants.html, (2005)
20. A. Schneuwly, P. Groning, L. Schlapbach, C.A.-I. Irrgang, C., and J.A.-V. Vogt, J., Breakdown behavior of oil-impregnated polypropylene as dielectric in film capacitors, Dielectrics and Electrical Insulation, IEEE Transactions on [see also Electrical Insulation, IEEE Transactions on], 5, (6), 862–868 (1998)
21. S. Kim, K. Yoshino, Dielectric Breakdown of High-Polymer Insulating Materials at Cryogenic Temperatures, Electrical Engineering in Japan, 106, (1), 1–7 (1986)
22. F.W. Billmeyer, Textbook of Polymer Science, 3rd ed, New York, John Wiley & Sons (1984)
23. J.R. Webster, Thin Film Polymer Dielectrics for High-Voltage Applications under Severe Environments, Electrical Engineering, Virginia Polytechnic Institute and State University (1998)
24. F. Bauer, Piezotech, Poly(vinylidene fluoride-trifluoroethylene-chlorotrifluoroethylene) terpolymer, http://www.piezotech.fr/, (2008)
25. K. Barbalace, EnvironmentalChemistry.com, Periodic Table of Elements Sorted by Eletronegativity, http://environmentalchemistry.com/yogi/periodic/electronegativity.html, (2007)
26. P. Moses, High Voltage Blocking Circuits for Permittivity Measurements http://www.personal.psu.edu/pjm112/PDF/BC.PDF, (2003)
27. P. Moses, Automated Polarization Measurement System, http://www.personal.psu.edu/pjm112/PDF/Pol_Strain.PDF, (2003)
28. M. Lines, A. Glass, Principles and Applications of Ferroelectric and Related Materials, Oxford, Clarendon Press (1977)
29. M. Dawber, I. Faman, and J.F. Scott, A Classroom Experiment to Demonstrate Ferroelectric Hysteresis, American Association of Physics Teachers, 71, (8), 819–822 (2003)
30. A.J. Gordon, R.A. Ford, The Chemist's Companion: A Handbook of Practical Data, Techniques, and References, Wiley (1973)
31. Thermo Scientific, Production Specification (NESLAB RTE and EX Series), http://www.thermo.com/eThermo/CMA/PDFs/Product/productPDF_25045.pdf, (2008)
32. DuPont, Material Safety Data Sheet (SUVA 404A), http://www.thermo.com/eThermo/CMA/PDFs/Various/File_26429.pdf, (2001)

Chapter 4

Experimental Results and Discussion

4.1 Introduction

In this chapter, the electrical properties of several polymer films including polypropylene (PP), polyimide (PI), polymethyl methacrylate (PMMA), and poly(vinylidene fluoride-trifluoroethylene-chlorotrifluoroethylene) terpolymer (p(VDF-TrFE-CTFE)), will be investigated. Low-field (<1X10^{-3}MV/cm) permittivity (ε_r) and dielectric loss (tanδ) were investigated as a function of frequency and temperature. High-field (>1MV/cm) permittivity was calculated using dielectric displacement measurements. The temperature dependence and level of breakdown strength were related to polymer type and thermal-structural behavior.

4.2 Low Field Permittivity and Dielectric Loss

The low field (<1X10^{-3}MV/cm) permittivity (ε_r) and dielectric loss (tanδ) of the various polymer films at room temperature were calculated from capacitance measurements. The properties will be presented in **4.2.1**. The Temperature dependence of the low-field permittivity and dielectric loss are discussed in **4.2.2**.

4.2.1 Relative Permittivity and Dielectric Loss at Room Temperature

The low-field permittivity (ε_r) and dielectric loss ($\tan\delta$) of the various polymer films at room temperature are discussed in this section. Experimental results and the reported values of the relative permittivity and dielectric loss in the polymer films at room temperature at 1kHz are listed in Table **4.1**. PP exhibited the lowest relative permittivity of 2 among all the polymer films being close to the reported value of 2.2 [1]. The reported relative permittivities of PI and PMMA were approximately 3.4 and 3.0 respectively [2], being slightly higher than the experimentally determined values of 2.8 and 3.7. The difference could be related to different polymer characteristics including molecular weight, crystallinity, etc. The reported value of relative permittivity was 50 for the p(VDF-TrFE-CTFE) terpolymer [3], with the experimentally determined value of 50.

The dielectric losses of PP, PI, PMMA, and the p(VDF-TrFE-CTFE) terpolymer were reported to be <0.5%, <0.5%, 5.5%, and 10% at 1kHz respectively [1–4]. PP and PI experimentally displayed loss values below 0.5% at 1kHz—these were the lowest values. PMMA exhibited a loss value of 4.0%. The p(VDF-TrFE-CTFE) terpolymer showed the highest dielectric loss: 10% at room temperature at 1kHz.

The low-field permittivity and dielectric loss calculated from the capacitance measurements were close to reported values as shown in Table **4.1**. The dipolar contribution can be estimated by subtracting the relative permittivity from the square of the refractive index of a material. PMMA had significant low-frequency polarizability. The relative permittivity and the dielectric loss increased with increasing polarity of the polymers, PP<PI<PMMA<P(VDF-TrFE-CTFE) terpolymer.

Table **4.1**: Comparison of relative permittivity (ε_r) and dielectric loss (tanδ) for the various polymer films at room temperature

Polymer	ε_r at 1kHz	tanδ at 1kHz (%)	Reported ε_r at 1kHz	Reported tanδ at 1kHz (%)	Refractive Index (n)
Polypropylene (PP)	~2.0	<0.5	2.2–2.3 [1]	<0.5 [4]	1.5 (n^2=2.3) [1]
Polyimide (PI)	~2.8	<0.5	~2.8 [5]	<0.5 [6]	1.7 (n^2=2.9) [2]
Polymethyl methacrylate (PMMA)	~3.7	~4.0	~3.0 [1]	~5.5 [1]	1.5 (n^2=2.3) [1]
P(VDF-TrFE-CTFE) terpolymer	~50	~10	~50 [3]	~10 [7]	-

4.2.2 Temperature Dependence of Relative Permittivity and Dielectric Loss

The temperature dependence of the polymer films' low-field permittivity (ε_r) and dielectric loss (tanδ) were also calculated from capacitance measurements as determined at various frequencies. PP displayed a slight decrease of relative permittivity with increasing temperature up to around 50°C as shown in Figure **4.1** (a). The slope of the relative permittivity in PP changed above 50°C. There was little effect in regard to the thermal-expansion coefficient (α_L) of PP. The relative permittivity slightly decreased with the thermal-expansion coefficient. Schneuwly et al. reported a structural change at around 50°C of PP using DSC (differential scanning calorimetry) measurements [8]. The decrease of relative permittivity can be related to the structural change of PP. The structural change will be discussed in **4.4.2**. Methyl groups in PP chains induce a low

dipole moment in the long chain molecule and might result in the low relative permittivity over the wide temperature range. The dielectric loss of PP was below 0.5% as displayed in Figure **4.1** (b).

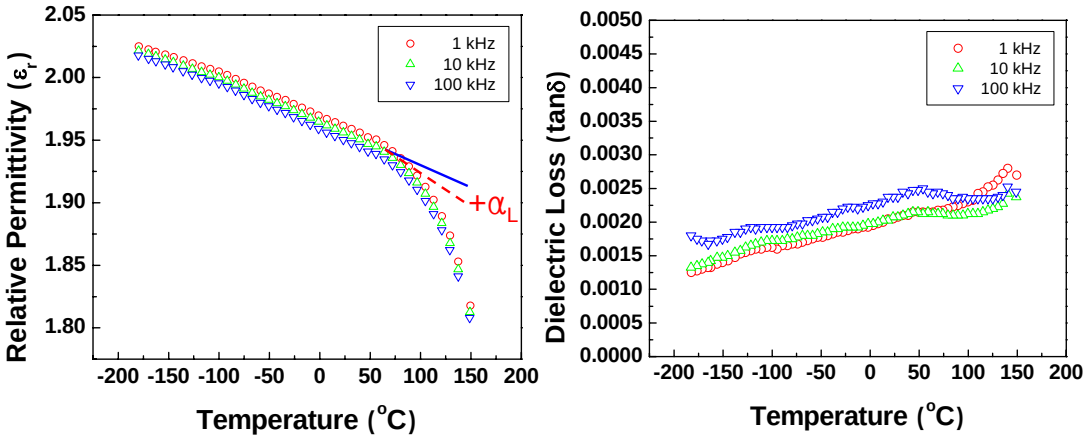

Figure **4.1**: Temperature dependence of low-field (a) permittivity (ε_r) and (b) dielectric loss (tanδ) of PP films

The temperature dependence of the low-field relative permittivity (ε_r) and the dielectric loss (tan δ) of PI are illustrated in Figure **4.2**. The relative permittivity slightly decreased with increasing temperature.

A peak was observed in the relative permittivity of PI with a corresponding peak in the dielectric loss at -40°C. Similar results have been reported by Melcher et al. in which different water contents in PI were explored [9]. The reported magnitude of the loss peak was proportional to water content and the loss peak. The loss peak attributed to water-molecule rotation is coupled with hydrogen bonding to the PI chains [9].

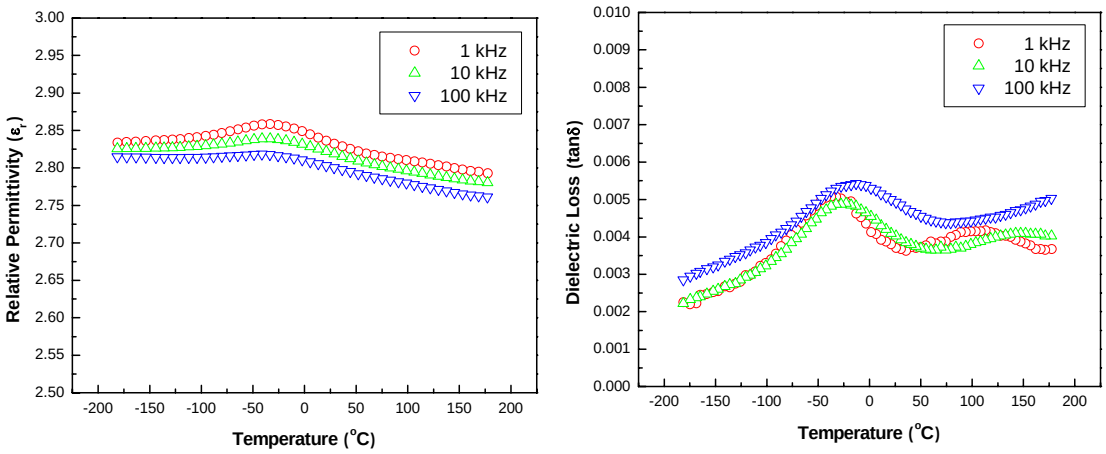

(a) (b)

Figure **4.2**: Temperature dependence of low-field (a) permittivity (ε_r) and (b) dielectric loss (tanδ) in PI

The low-field permittivity (ε_r) of PMMA as a function of temperature and frequency is shown in Figure **4.3** (a). The value of the low-field permittivity increased with increasing temperature and decreasing frequency. The low-field permittivity of PMMA is higher than that of PP and PI. As discussed in Chapter **3**, PMMA has a polar side-chain structure and its permittivity is expected to increase as chain-mobility increases. The dielectric loss (tanδ) of PMMA at 1kHz in Figure **4.3** (b) has loss peaks at 0°C and 75°C. The low-temperature peak is related to side-chain motion (β-relaxation) and the high-temperature peak is related to the back-bone motion (α-relaxation) [10]. Both α and β relaxations are temperature- and frequency-dependent up to the T_g of 105°C.

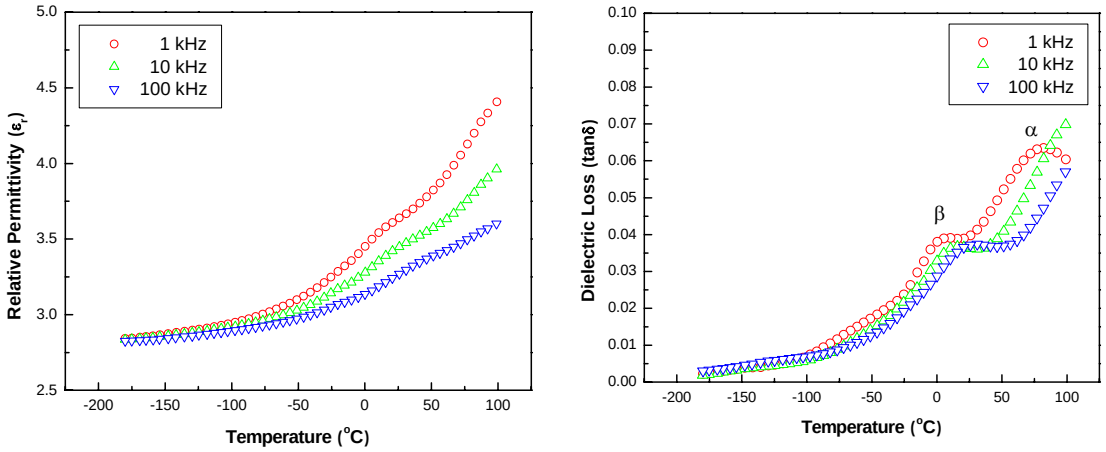

Figure **4.3**: Temperature dependence of low-field (a) permittivity (ε_r) and (b) dielectric loss (tanδ) of PMMA

The temperature dependence of low-field permittivity (ε_r) and dielectric loss (tanδ) of the p(VDF-TrFE-CTFE) terpolymer is depicted in Figure **4.4**. The terpolymer exhibited an increase in the relative permittivity and dielectric loss at around -10°C. This could be related to T_g and a phase transition of the terpolymer. The relative permittivity of the terpolymer was more dependent on temperature and frequency than that of other polymers, as shown in Figure **4.4** (a). The terpolymer showed typical ferroelectric frequency-dependent relaxor behavior. The relative permittivity of the terpolymer strongly increased with increasing temperature up to around 40°C; it then decreased. The maximum relative permittivity of the terpolymer was around 40–50. This ferroelectric polymer showed much higher low-field relative permittivity than PP, PI, and PMMA. The high relative permittivity is due to a high dipole moment that was induced by fluorine and chlorine atoms in the terpolymer chains.

The dielectric loss of the p(VDF-TrFE-CTFE) terpolymer was also strongly dependent on temperature and frequency, as illustrated in Figure **4.4** (b). The dielectric loss increased up to around room temperature, and then it decreased. The maximum dielectric loss was about 45% around room temperature at 100kHz. The dielectric loss of 45% is very high for polymers. The frequency dispersion of the dielectric loss in the terpolymer was also observed. The observed frequency dispersion of the terpolymer has also been reported by Lu, Bauer, et al. [3, 11].

Relative permittivity and dielectric loss increased sharply at around -10°C with increasing temperature. This can be related to β relaxation, which indicates a glass transition of terpolymer chains in an amorphous phase [12]. The glass transition in the amorphous phase and the reorientation of nano-clusters in a crystalline phase of the terpolymer influences the increase of relative permittivity and dielectric loss at -10°C [12].

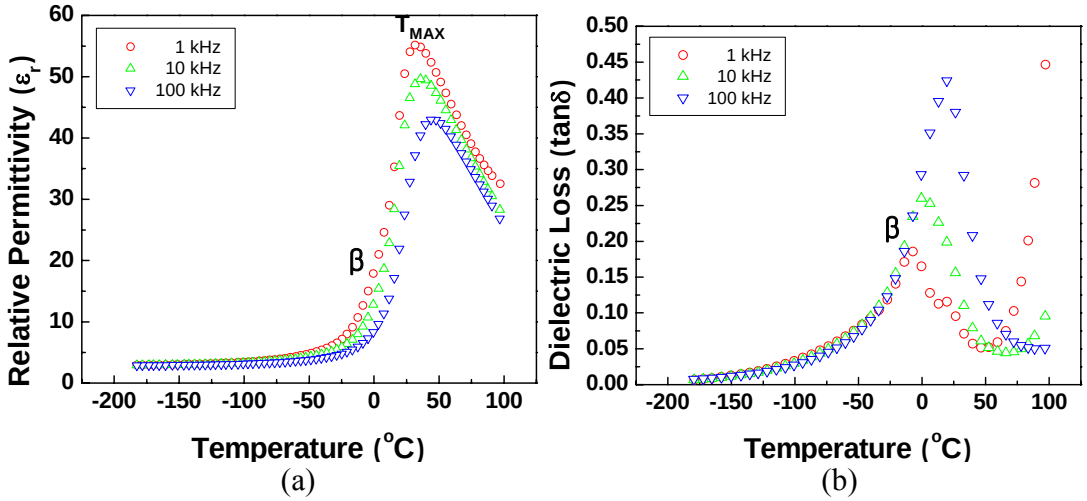

Figure **4.4**: Temperature dependence of low-field (a) permittivity (ε_r) and (b) dielectric loss (tanδ) of p(VDF-TrFE-CTFE) terpolymer

4.3 High-field Permittivity

The high-field (>1MV/cm) permittivities (ε_r) of PP, PI, and PMMA films were found at room temperature, as depicted in Figure **4.5**. The polymers including PP, PI, and PMMA exhibited linear dielectric behavior in regard to the polarization-electric field (P-E). P(VDF-TrFE-CTFE) terpolymer films exhibited a relative permittivity with the highest value of the various polymers. The higher relative permittivity of the terpolymer, which is a ferroelectric polymer, was related to the non-linear response of the P-E. An area within the P-E indicates dielectric loss ($\tan\delta$). The terpolymer displayed higher high-field dielectric loss with a larger area within the P-E than did other polymers. This behavior was the same as shown in higher low-field dielectric loss of the terpolymer than that of PP, PI, and PMMA in **4.2.1**. This higher low-field dielectric loss may be the result of the higher dipole moment induced by the fluorine and chlorine atoms in the terpolymer than that derived from methyl, phenyl, and methacrylate groups in PP, PI, and PMMA.

The high-field results show that PP, PI, and PMMA are linear dielectrics and that the energy density can be determined from Equation **1.7** ($E_{vol} = \frac{1}{2}\varepsilon_o \varepsilon_r E_{Br}{}^2 \cong \frac{1}{2} C V_m^2 \times \frac{1}{Ad}$). The p(VDF-TrFE-CTFE) terpolymer is a non-linear dielectric and the energy density is defined by the relationship given in Equation **1.6** ($U_e = \int E dD$).

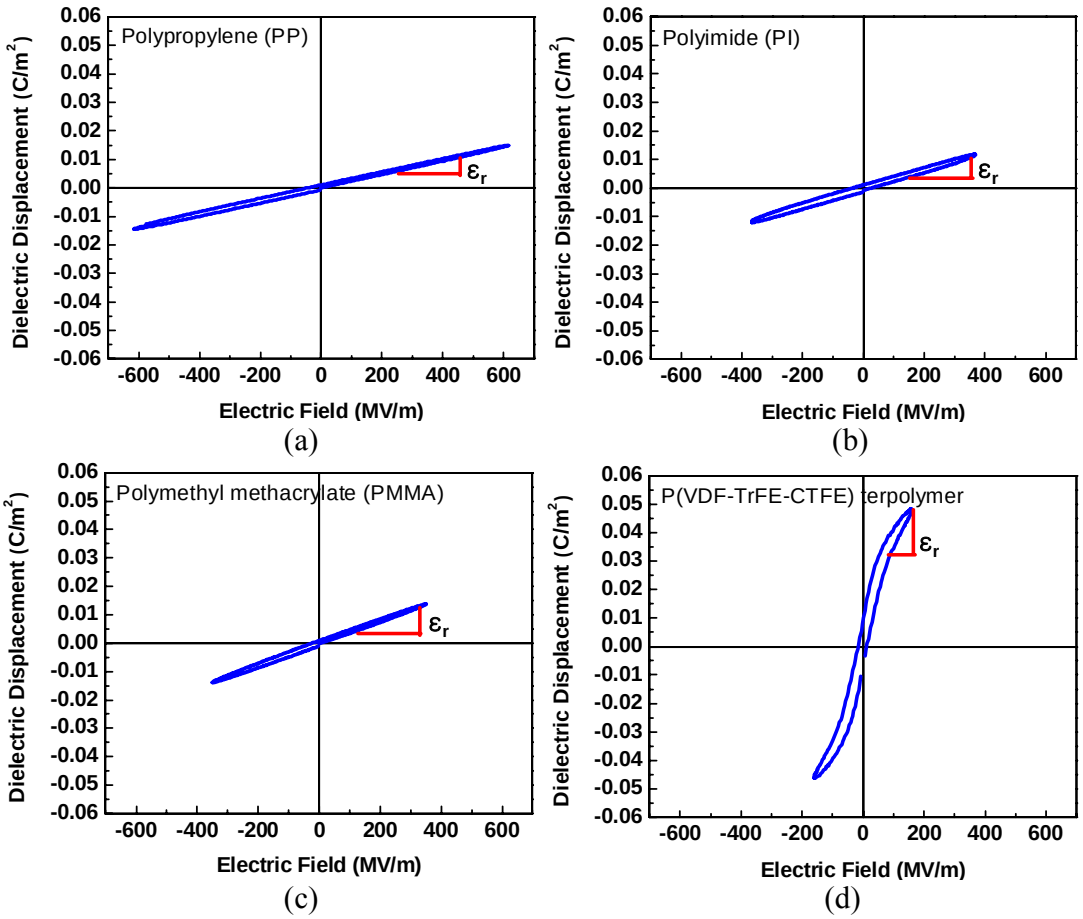

Figure **4.5**: Dielectric displacement of various polymer films including (a) PP, (b) PI, (c) PMMA, and (d) p(VDF-TrFE-CTFE) terpolymer at room temperature

4.4 Dielectric Breakdown in Polymers

The breakdown strength of the various polymer films including PP, PI, PMMA, and the p(VDF-TrFE-CTFE) terpolymer will be discussed in the following sections. The confidence of measured data in the polymer films was estimated using Weibull distributions. Breakdown strength in the polymer films will be introduced over a wide

temperature range and related to the temperature dependence and structural/thermal properties of the various polymers.

4.4.1 Dielectric Breakdown of Polymer Films at Room Temperature

The dielectric breakdown of the various polymer films was investigated at room temperature. Trough and mushroom holders, as discussed in Chapter 4, were used to investigate the effect of holder configuration. The results of the different holders were found to be similar. All the breakdown measurements of the various polymer films were done using the mushroom holder. PP exhibited a dielectric-breakdown strength of 7.6 MV/cm; this was the highest value among the polymers at room temperature as listed in Table **4.2**. PI and PMMA displayed relatively high breakdown strengths of 6.0 and 6.5 respectively, at room temperature. The p(VDF-TrFE-CTFE) terpolymer exhibited a breakdown strength of 2.5 MV/cm, which was the lowest of all the polymers. All investigated polymers showed similar breakdown strengths as compared to reported values. Polar polymers generally display higher breakdown strengths than non-polar polymers because of the former's higher dipole moment [13]. However, PP, a non-polar polymer, displayed the highest breakdown strength at room temperature. One of the reasons for PP having the highest breakdown strength might be related to the experiment's use of electrodes: Aluminum electrodes were commercially deposited on the PP films using evaporation at a low temperature (~ -10°C). On the other hand, platinum electrodes were deposited on the other polymers using sputtering without

cooling. The polymer films might be damaged during the sputtering. It is one possible reason for the breakdown strength of PI and PMMA being lower than that of PP.

Table **4.2**: Room temperature breakdown strengths of the various polymer dielectrics

Polymer	Breakdown Strength (MV/cm)	Reported Breakdown Strength (MV/cm)
PP	7.6	~6.4 [8]
PI	6.0	~4.0 [14]
PMMA	6.5	~10 [13]
P(VDF-TrFE-CTFE) terpolymer	2.5	1.0–3.5 [15]

The breakdown strength of the polymer films was analyzed using Weibull distributions to estimate the reliability and the quality of the polymer films [16]. The Weibull distributions of breakdown in the polymer films at room temperature are depicted in Figure **4.6**. The β value of PP was found to be much higher at room temperature than that of the other polymers including PI, PMMA, and the p(VDF-TrFE-CTFE) terpolymer. The β value of PP was also relatively higher than that of other samples over a wide temperature range. The high β value indicates little spread in data, providing a high degree of confidence. The effect of the quality of contacts between the Pt electrodes and the polymer films may have resulted in the lower β of the samples. Breakdown data follow Gaussian distributions when the β value is 3. All the polymer films showed higher β values than 3, and this can be considered as evincing a high degree of reliability.

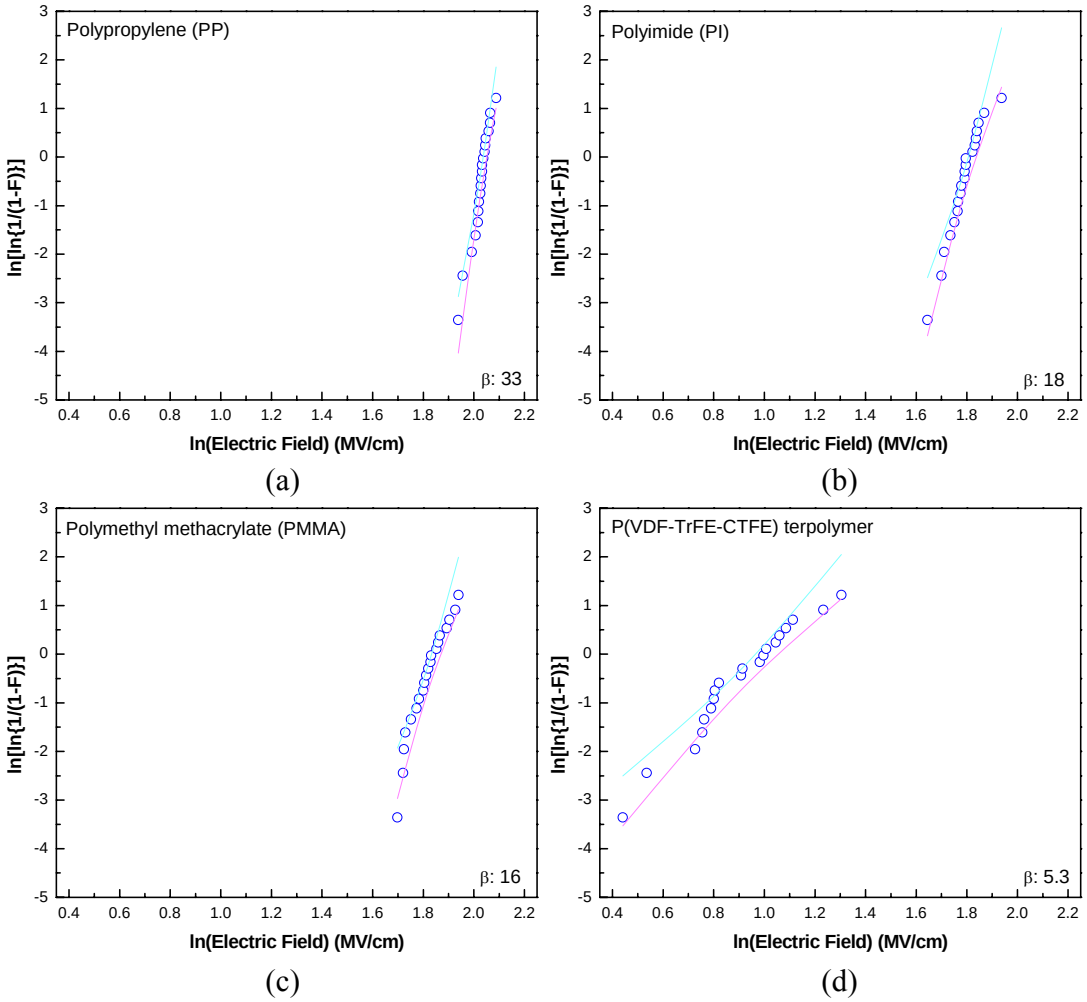

Figure **4.6**: Weibull distribution of breakdown in various polymer films at room temperature including (a) PP, (b) PI, (c) PMMA, and (d) p(VDF-TrFE-CTFE) terpolymer

4.4.2 Temperature Dependence of the Breakdown Strength of Polymer Films

The breakdown strength of all the polymer films increased with decreasing temperature. The decrease of breakdown strength with increasing temperature in polymers is related to various dielectric breakdown mechanisms such as thermal, electromechanical, free-volume, and electronic avalanche as discussed in Chapter 2 [13].

More than one breakdown mechanism may affect dielectric breakdown [16]. A primary goal of this work was to survey the temperature dependence of the dielectric breakdown of a variety of polymers and to connect the breakdown behavior to structural changes.

The temperature-dependent dielectric-breakdown behavior of all of the polymers is shown in Figure **4.9**. The error bars on each plot (a, b, c, and d) are one standard deviation, assuming a Gussian distribution. Weibull distributions with $\beta>3.0$ can be approximated by a Gaussian distribution, and all of the data shown in Figure **4.6** have β values greater than 5.0.

The dielectric breakdown at liquid nitrogen (liq. N_2) temperature was explored for PP, PMMA, and P(VDF-TrFE-CTFE). The breakdown was lower than or equal to the next highest temperature for all breakdown tests at liquid nitrogen temperature as shown in Figure **4.9**. There were several challenges in dielectric breakdown testing with liq. N_2. First, the samples become very brittle, making problematic mechanical fracture under electrostatic stress becomes more frequent. The mechanical failure is especially critical for the mushroom holder. Second, bubbles were always observed in the liq. N_2 and were perhaps initiators for dielectric breakdown. Because of these potential effects, dielectric breakdown at liq. N_2 temperature will not be discussed.

The temperature dependence of breakdown strength for PP is shown in Figure **4.9** (a). The dielectric-breakdown data exhibited the smallest error among all the polymers, and only subtle changes in the temperature-dependent dielectric breakdown behavior were observed. For PP, there was a linear decrease of dielectric-breakdown strength with temperature, except within the 50°C–100°C temperature range. The dip in breakdown strength corresponds with a slight change in the relative permittivity above 50°C in

Figure **4.1**. Schneuwly et al. also found that PP showed a slight change in breakdown strength at 50°C. This slight change was investigated using DSC measurements and considered that additives or other impurities may exist in the amorphous region of PP [8]. These additives can introduce additional free volume in an amorphous region of PP with increasing temperature as polymer softens. This structural change in PP results in the observed decrease in breakdown strength. The decrease in breakdown strength at 140°C could be related to the melting point of PP, which is around 165°C. Electromechanical breakdown may be dominant at this temperature. At temperatures (>140°C), PP films become very soft and experience a compressive stress between electrodes. The pressure increases and the thickness of the PP films decreases with increases in the applied electric field. The PP films receive more stress and charges as the thickness of the PP films decreases continuously. Finally, dielectric breakdown occurs.

The dielectric breakdown strength in PI from room temperature to 175°C is shown in Figure **4.9** (b); the results are consistent with those of Kim et al., who reported breakdown strength values of PI between 5 and 6 MV/cm [14]. In the case of PI, a slight change in breakdown occurred around 130°C as shown in Figure **4.9** (b), being well below the glass-transition temperature (T_g=230°C–260°C). The increase of the breakdown strength in PI below room temperature has been reported by Kim et al.; it was found to be independent of temperature up to 27°C [14]. The results of this thesis show no change in breakdown strength up to 100°C. The decrease in dielectric-breakdown strength between 100°C and 130°C is statistically significant, based on our analysis of 20 samples per temperature. The result is surprising because no significant structural or

dielectric changes occurs at below 200°C [9]. The dielectric data in Figure **4.2** (b) suggests that water is entrained in the PI structure, which may influence properties above 100°C. Fujita et al. reported differential scanning calorimetry (DSC) data of PI with various water contents as shown in Figure **4.7** [17]. Data for all the water contents showed a thermal absorption peak at around 110°C, which corresponds with the decrease in breakdown strength for PI [17]. The water content in PI decreased with increasing time to dry, giving a lower peak of thermal absorption in DSC [17]. Thermogravimetric analysis (TGA) data for the PI samples used in this research is displayed in Figure **4.8**. The data also exhibited a change in weight percent for PI at around 100°C. These results indicate that water continues to evolve from the PI until around 100°C; the results also support the decrease in breakdown strength of PI at around 100°C. It is speculated that there is a rapid removal of water from the PI as it is immersed in the dielectric fluid at high temperature for the breakdown test. The rapid evolution of water will have a significant impact on the structure and dielectric breakdown strength of PI.

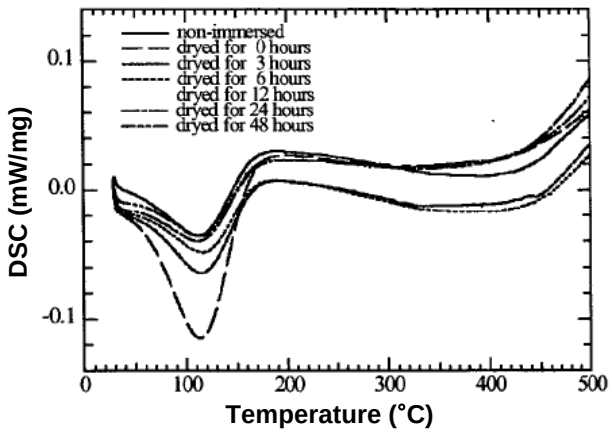

Figure **4.7**: Differential scanning calorimetry (DSC) data for PI with various water contents [17]

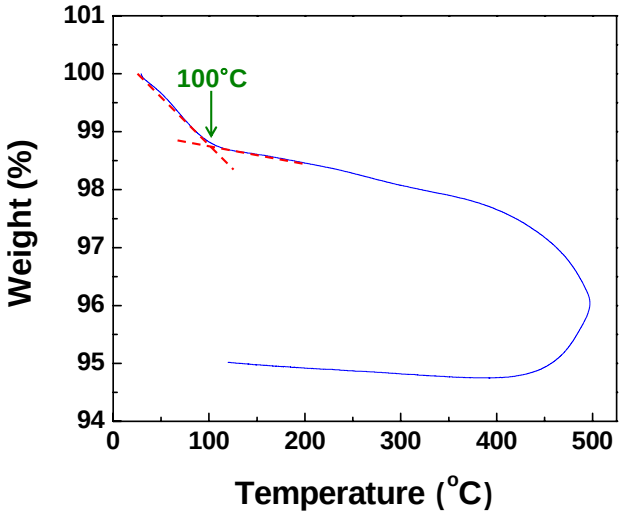

Figure **4.8**: Thermogravimetric analysis (TGA) data for PI which shows a change in weight percent with changing temperature

The breakdown strength of PMMA was investigated as a function of temperature. Large error bars were found for temperatures <0°C as shown in Figure **4.9** (c); this was attributed to sample handling and the brittle nature of the polymer. PMMA shows an increase in the dielectric breakdown strength as temperature increases from -150°C to -100°C and then there is a monotonic decrease in the breakdown strength as the temperature increased to 75°C. The decrease in breakdown strength with increasing temperature could be related to α and β relaxations, which corresponded with that of dielectric loss for PMMA. Among all of the polymers, PMMA exhibited the highest breakdown strength in the low-temperature region in this study.

The breakdown strength of the p(VDF-TrFE-CTFE) terpolymer increased with decreasing temperature as with the other polymers. The terpolymer showed a change in breakdown strength at around -10°C, as presented in Figure **4.9** (d). This could be related to T_g and a β relaxation of the terpolymer, which occurs in the range of -20°C to -10°C.

Breakdown strength decreased at around -100°C with decreasing temperature for PP, PMMA, and the p(VDF-TrFE-CTFE) terpolymer, as shown in Figure **4.9** (a), (c), and (d). This decrease could be related to brittleness of the polymers, which generally increases with decreasing temperature. Electrostatic attraction between the brittle polymers and the curved copper-dome electrode on the mushroom holder might cause cracks in the polymer films. The cracks, in turn, could result in a decrease in breakdown strength.

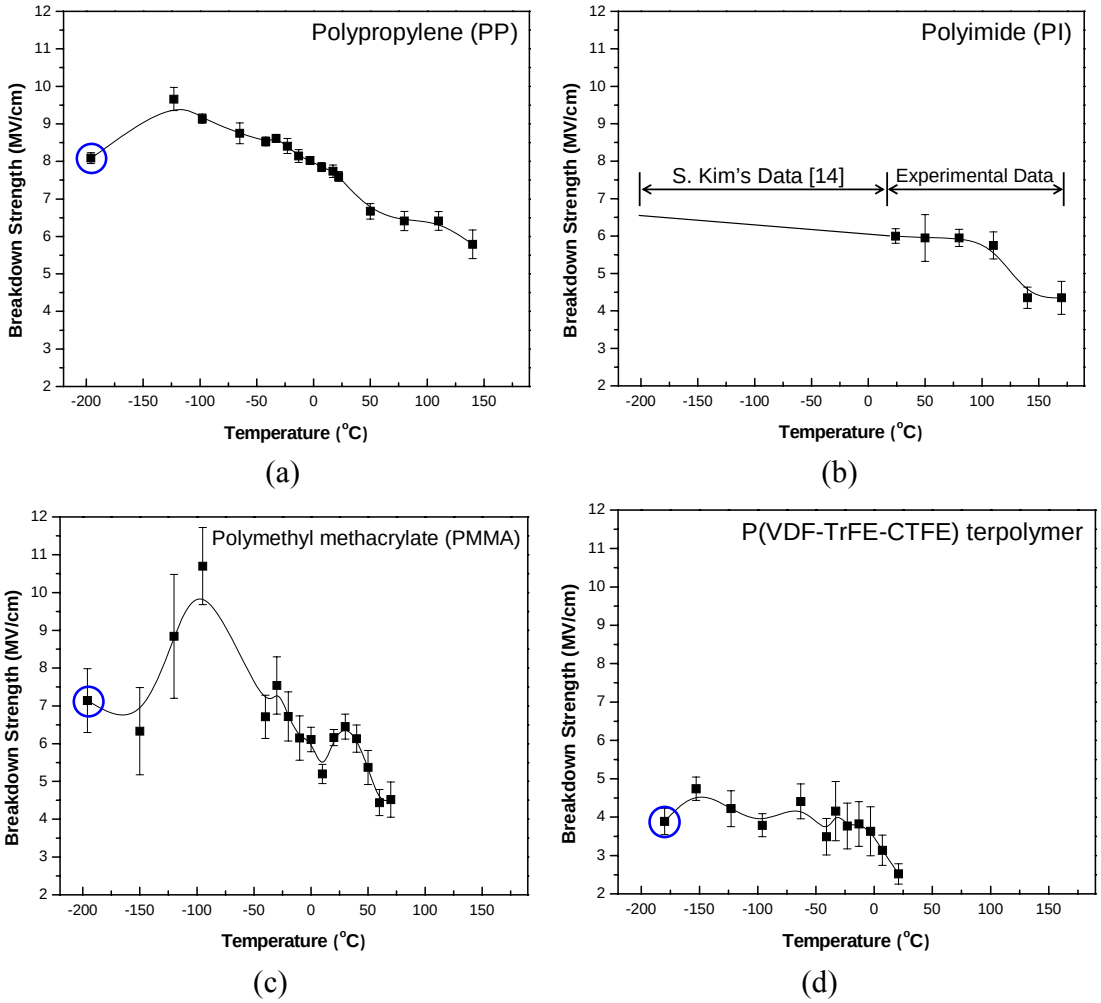

Figure **4.9**: Temperature dependence of breakdown strength in various polymer films including (a) PP, (b) PI [14], c) PMMA, and (d) p(VDF-TrFE-CTFE) terpolymer. Circles (○) indicate breakdown data using liquid nitrogen

4.5 Energy Density

Maximum energy per unit volume can be calculated using Equation **1.7** ($E_{vol} = \frac{1}{2}\varepsilon_o \varepsilon_r E_{Br}^{\ 2}$). The energy densities of the various polymers at maximum breakdown strength (E_{Br}) are listed in Table **4.3**. PMMA showed the highest energy density because of it had the highest breakdown-strength value at -95°C. In the linear polymer dielectrics, PMMA, a polar polymer, exhibited higher energy density than the non-polar polymers, PP and PI. This result shows that higher energy density can be achieved from higher polar polymers.

Table **4.3**: Maximum energy density of various polymers at the maximum breakdown strength

Polymer	ε_r at 1kHz	Max. E_{Br} (MV/cm)	Max. E_{vol} (J/cm^3)
Polypropylene	2.0	9.0 at -98°C	7.2
Polyimide	2.8	6.0 at RT	4.5
Polymethyl methacrylate	2.8	11 at -95°C	15
P(VDF-TrFE-CTFE) terpolymer	4.0	4.0 at -63°C	2.8

References

1. J. Brandrup, E.H. Immergut, Polymer Handbook, 3rd ed, New York, Wiley (1989)
2. Good Fellow, Technical Data – Material Properties, http://www.goodfellow.com/csp/active/gfHome.csp, (2008)
3. Y. Lu, J. Claude, B. Neese, Q. Zhang, and Q. Wang, A Modular Approach to Ferroelectric Polymers with Chemically Tunable Curie Temperatures and Dielectric Constants, J. Am. Chem. Soc., 128, (25), 8120–8121 (2006)
4. J. Strydom, Dielectric Measurements for Power Electronic Applications, in IEEE transactions on industry applications, 829 (2001)
5. Clipper Controls, Dielectric Constant Reference Guide, http://www.clippercontrols.com/info/dielectric_constants.html#L, (2008)
6. G. Xu, C.C. Gryte, A.S. Nowick, S.Z. Li, Y.S. Pak, and S.G. Greenbaum, Dielectric relaxation and deuteron NMR of water in polyimide films, Journal of Applied Physics, 66, (11), 5290–5296 (1989)
7. Y. Lu, J. Claude, B. Neese, Q. Zhang, and Q. Wang, Supporting Information: A Modular Approach to Ferroelectric Polymers with Chemically Tunable Curie Temperatures and Dielectric Constants, The Pennsylvania State University (2006)
8. A. Schneuwly, P. Groning, L. Schlapbach, C.A.-I. Irrgang, C., and J.A.-V. Vogt, J., Breakdown behavior of oil-impregnated polypropylene as dielectric in film capacitors, Dielectrics and Electrical Insulation, IEEE Transactions on [see also Electrical Insulation, IEEE Transactions on], 5, (6), 862–868 (1998)
9. J. Melcher, Y. Daben, and G. Arlt, Dielectric Effects of Moisture in Polyimide, IEEE Transactions on Dielectrics and Electrical Insulation, 24, (1), 31–38 (1989)
10. R. Bergman, F. Alvarez, A. Alegria, and J. Colmenero, Dielectric Relaxation in PMMA Revisited, Journal of Non-Crystalline Solids, 235, (237), 580–583 (1998)
11. F. Bauer, E. Fousson, Q.M. Zhang, and L.M.A.-L. Lee, L.M., Ferroelectric copolymers and terpolymers for electrostrictors: synthesis and properties, Dielectrics and Electrical Insulation, IEEE Transactions on [see also Electrical Insulation, IEEE Transactions on], 11, (2), 293–298 (2004)
12. S.H. Zhang, C. Huang, R.J. Klein, F. Xia, D. Jeong, K.L. Ren, Q.M. Zhang, and F. Bauer, Dynamics in Relaxor Ferroelectric Polymers, 2004 IEEE International Ultrasonics, Ferroelectrics, and Frequency Control Joint 50th Anniversary Conference, 138–142 (2004)
13. M. Ieda, M. Nagao, and M. Hikita, High-field Conduction and Breakdown in Insulating Polymers, IEEE Transactions on Dielectrics and Electrical Insulation, 1, 934–945 (1994)
14. S. Kim, K. Yoshino, Dielectric Breakdown of High-Polymer Insulating Materials at Cryogenic Temperatures, Electrical Engineering in Japan, 106, (1), 1–7 (1986)
15. J. Claude, Y. Lu, K. Li, and W. Wang, Electrical Storage in Poly(vinylidene fluoride) based Ferroelectric Polymers: Correlating Polymer Structure to Electrical Breakdown Strength, American Chemical Society, 20, (6), 2078–2080 (2008)

16. T. Blythe, D. Bloor, Electrical Properties of Polymers, 2nd ed, New York, Cambridge University Press (2005)
17. S. Fujita, Y. Kamei, Electrical Properties of Polyimide with Water Absorption, 11th International Symposium on Electrets, 2002, 275–278 (2002)

Chapter 5

Conclusion and Future Work

5.1 Conclusion

The electrical properties of several polymer films including polypropylene (PP), polyimide (PI), polymethyl methacrylate (PMMA), poly(vinylidene fluoride-trifluoroethylene-chlorotrifluoroethylene), and terpolymer (p(VDF-TrFE-CTFE)) were investigated. The results are summarized in Figure **5.1**.

The results shown in Table **5.1** reveal some trends in the dielectric permittivity and breakdown data. First, the relative polarity of the polymers can be qualitatively compared. Guided by the discussion around Figure **1.2**, the electronic contribution of the dielectric polarization is related to the index of refraction (n). The dipolar contribution can be estimated by subtracting the 1kHz permittivity from n^2. As can be seen from the data in Figure **5.1**, PMMA and p(VDF-TrFE-CTFE) have significant low-frequency polarizability, and PP and PI have solely electronic polarizability. As indicated in the discussion in Chapter **1**, the dielectric breakdown strength can be correlated to polarizability and is probably why PMMA had the highest breakdown strength in the low-temperature region. PP and PI had lower breakdown values, and p(VDF-TrFE-CTFE) was a lab-grade sample with a large number of extrinsic defects. In the linear polymer dielectrics, the polar polymer PMMA exhibited higher energy density than the non-polar polymers PP and PI.

Table **5.1**: Electrical properties of various polymer dielectrics

Polymer	Low Field ε_r at RT at 1kHz	Low Field tanδ at RT at 1kHz (%)	Maximum Breakdown Strength (MV/cm)	Maximum Energy Density (J/cm^3)
Polypropylene	~2.0	<0.5	9.0 at -98°C	7.2
Polyimide	~2.8	<0.5	6.0 at RT	4.5
Polymethyl methacrylate	~3.7	~4.0	11 at -95°C	15
P(VDF-TrFE-CTFE) terpolymer	~50	~10	4.0 at -63°C	2.8

The temperature-dependent dielectric breakdown strength of all of the polymers is summarized in Figure **5.1**. All of the polymers exhibited a general decrease in breakdown field with increasing temperature. There are some specific features in individual polymers that are related to the dielectric properties. PP exhibited a significant change in breakdown strength at 50°C, which was related to a structural change in the polymer [1]. The change in dielectric properties is correlated to the change in breakdown strength as shown in Figure **5.1** (a). PI exhibited a slight change in breakdown strength at around 130°C. The change could be related to water entrained in the PI structure, which may influence properties above 100°C. PMMA exhibited a much larger decrease in breakdown strength with temperature than the non-polar polymers, PI and PP. PMMA undergoes α and β relaxations before the T_g (=~105°C) is reached; this suggests a correlation of breakdown strength with increased side-group and chain mobility. The p(VDF-TrFE-CTFE) terpolymer displayed a large drop in breakdown strength at T_g and a β relaxation at around -10°C.

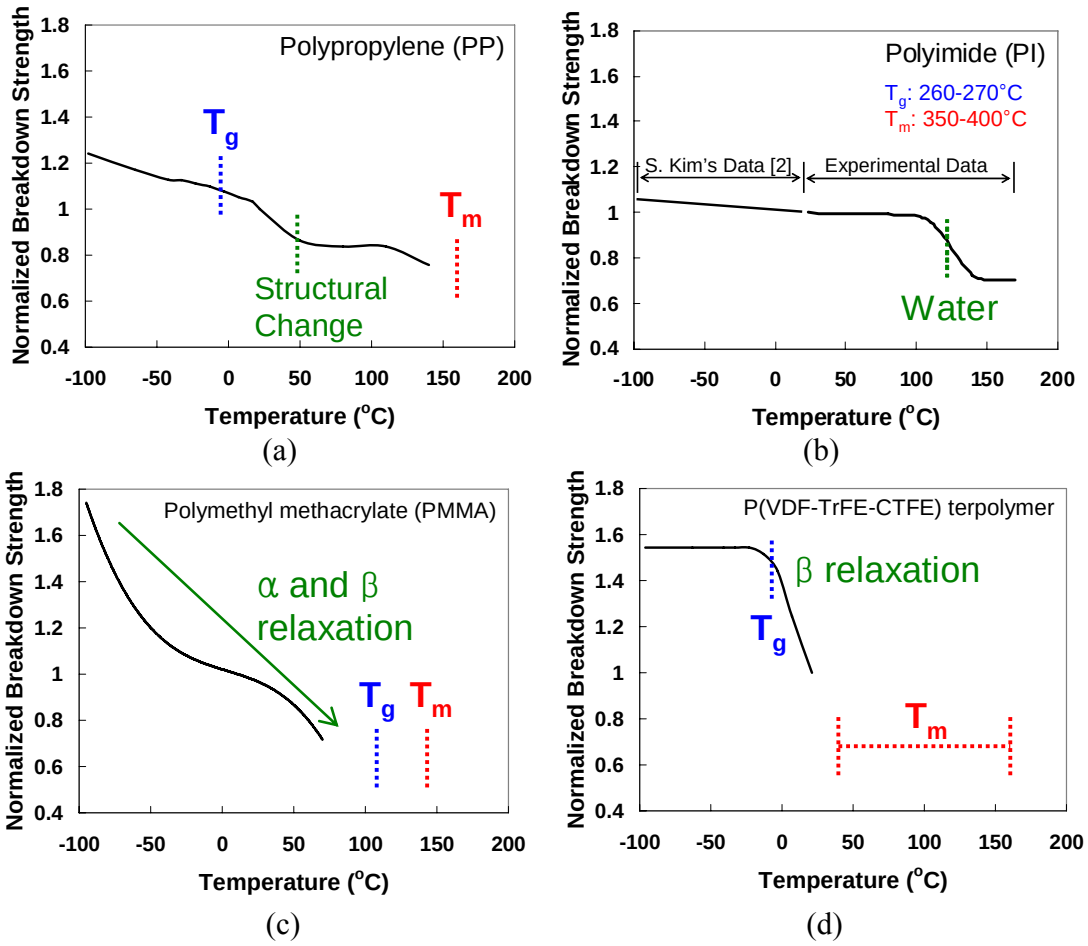

Figure **5.1**: Normalized breakdown strength of various polymer films including (a) PP, (b) PI [2], (c) PMMA, and (d) P(VDF-TrFE-CTFE) terpolymer

5.2 Future Work

Electrode effects in electrical properties should be investigated. Materials and deposition conditions of electrodes may influence the electrical properties of polymer dielectrics.

The breakdown strength of polymers can increases with reducing effects of the temperature dependence in breakdown strength. Minimizing impurities and relaxation, and controlling T_g and crystallinity of polymers are among the methods that may reduce to reduce temperature dependence.

Decrease in breakdown strength below -100°C will be prevented using other experimental setups. Bubbles from liquid nitrogen and cracks from electrostatic attraction in the low-temperature region can be avoided by using the new experimental setups. S. Kim et al. introduced an experimental setup for low-temperature breakdown measurements that can reduce the effects of bubbles and cracks as depicted in Figure **5.2** [2].

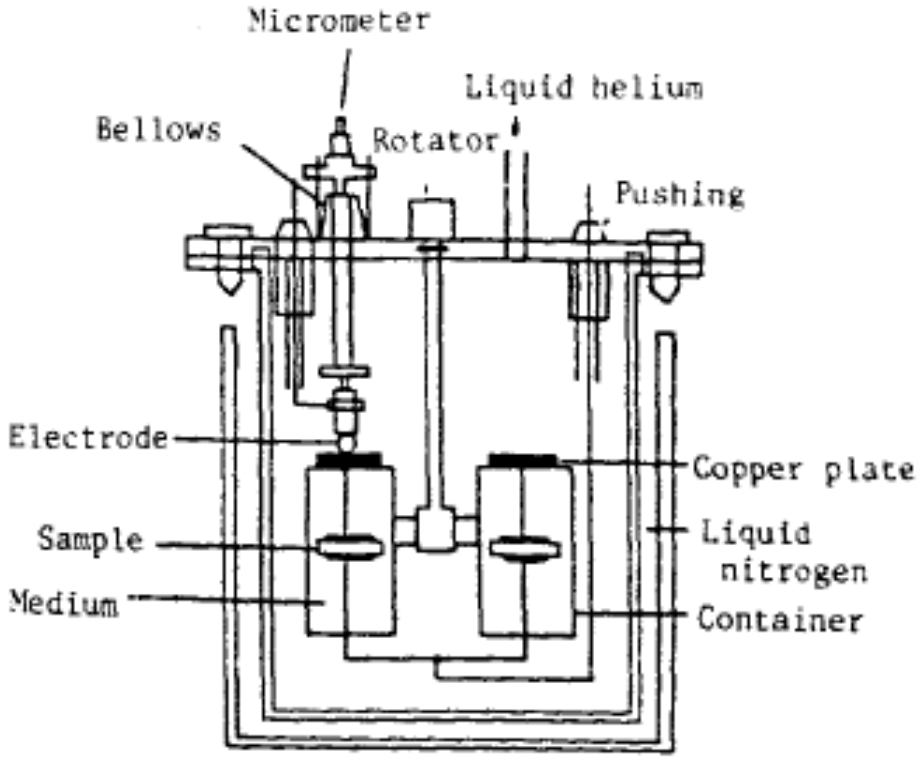

Figure **5.2**: Experimental setup for low-temperature breakdown measurements [2]

Ramp rate and thickness-dependence of breakdown strength in polymers should be studied. Such studies will be useful for understanding the breakdown mechanisms of polymer dielectrics.

Energy density can be enhanced by designing optimum polymers. The design of optimum polymers is suggested in Figure **5.3**. Polar/linear polymers in relation to cohesive energy density should be used to achieve a level of breakdown strength (E_{Br}). The temperature dependence of breakdown strength in polymers can be prevented by eliminating impurities, avoiding dielectric relaxations, and achieving a high T_g.

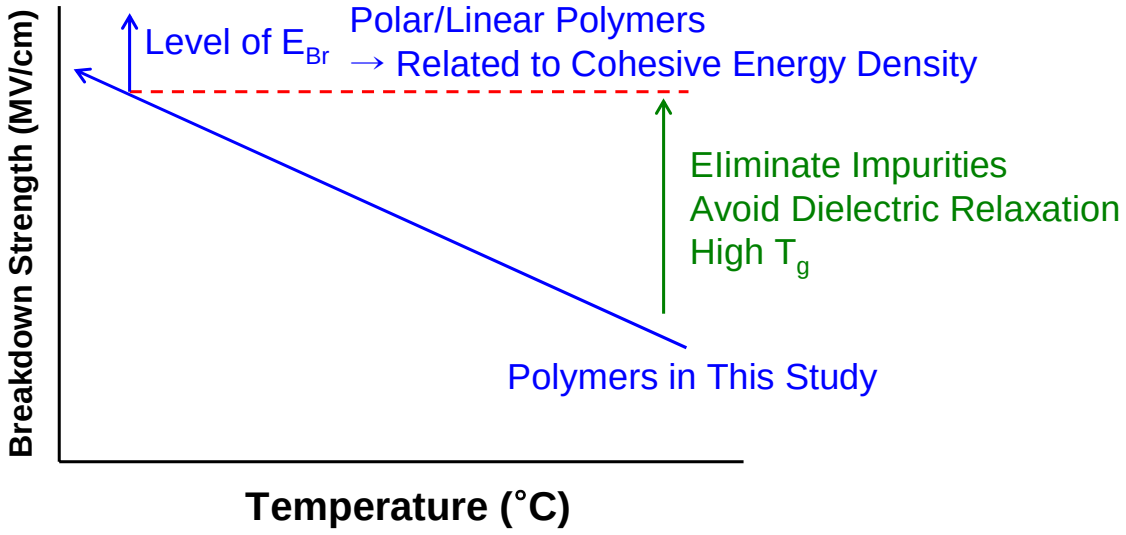

Figure **5.3**: Design of optimum polymers to enhance energy density

References

1. A. Schneuwly, P. Groning, L. Schlapbach, C.A.-I. Irrgang, C., and J.A.-V. Vogt, J., Breakdown behavior of oil-impregnated polypropylene as dielectric in film capacitors, Dielectrics and Electrical Insulation, IEEE Transactions on [see also Electrical Insulation, IEEE Transactions on], 5, (6), 862–868 (1998)
2. S. Kim, K. Yoshino, Dielectric Breakdown of High-Polymer Insulating Materials at Cryogenic Temperatures, Electrical Engineering in Japan, 106, (1), 1–7 (1986)